

Perspective

The Merging of Biological and Electronic Circuits

Jonathan J.Y. Teo^{1,2,4} and Rahul Sarpeshkar^{3,*}

SUMMARY

Biological circuits and systems within even a single cell need to be represented by large-scale feedback networks of nonlinear, stochastic, stiff, asynchronous, non-modular coupled differential equations governing complex molecular interactions. Thus, rational drug discovery and synthetic biological design is difficult. We suggest that a four-pronged interdisciplinary approach merging biology and electronics can help: (1) The mapping of biological circuits to electronic circuits via quantitatively exact schematics; (2) The use of existing electronic circuit software for hierarchical modeling, design, and analysis with such schematics; (3) The use of cytomorphic electronic hardware for rapid stochastic simulation of circuit schematics and associated parameter discovery to fit measured biological data; (4) The use of bio-electronic reporting circuits rather than bio-optical circuits for measurement. We suggest how these approaches can be combined to automate design, modeling, analysis, simulation, and quantitative fitting of measured data from a synthetic biological operational amplifier circuit in living microbial cells.

INTRODUCTION

Biological networks are notoriously difficult to analyze and interpret because they comprise tens of thousands of biochemical pathways that are linked. Pathways that are studied in isolation seldom provide deep insights into the behaviors of larger networks because they do not account for the complex interactions between pathways. In medicine, such systems biology interactions are important for drug or drug cocktail discovery based on pathway analysis. They are necessary for predicting drug or drug cocktail efficacy, safety, side effects, mechanism and site of action, and changes in cocktail composition or dosage with changing symptoms.

Molecular interactions manifest in several forms. For example, they can include resource limitations, which couple biochemical reactions that share the same enzyme or molecule; loading or non-modular effects that change the behavior of pathways depending on their downstream and upstream connections (Cardinale and Arkin, 2012); cross-talk between pathways caused by synergistic or antagonistic effects of transcription and translation regulation (Mukherji and Van Oudenaarden, 2009; Zeng et al., 2018) or by molecules having multiple fan-out interactions with downstream targets; feedback effects from interactions that form a closed loop between upstream and downstream molecules (Ferrell, 2002). To compound these difficulties, biochemical reactions are generally non-linear and noisy () such that simplified biological models that assume linear and/or deterministic interactions are not accurate.

One solution adopted by synthetic biologists is to fit biological circuits into neat computational blocks defined by logic gates. This digital framework has seen some successes in designing small biological circuits that use a relatively small number of logic gates. For example, Ausländer et al. built a 1-bit adder in a mammalian system using over 20 logic gates distributed among 9 different cell types (Ausländer et al., 2018). So far, it has proven difficult to scale these circuits to larger networks due to issues such as resource limitations including metabolic burden, loading and non-modularity, stochastics (noise), cross-talk, and feedback (Sarpeshkar, 2014; Teo et al., 2015).

Bio-molecular reactions are analog and stochastic by nature, so a blanket solution that treats all reactions like logic gates works optimally only in special cases such as memory storage and decision-making where deterministic digital behavior is appropriate. Additionally, an analog approach offers resource (molecular

¹Computational and Systems Biology Program at the Massachusetts Institute of Technology, Cambridge, MA 02139, USA

²Thayer School of Engineering, Dartmouth College, Hanover, NH 03755, USA

³Departments of Engineering, Microbiology & Immunology, Physics, and Molecular and Systems Biology, Dartmouth College, Hanover, NH 03755, USA

⁴Present address: Genome Institute of Singapore, Agency for Science, Technology and Research, 138672 Singapore

*Correspondence: rahul.sarpeshkar@dartmouth.edu
<https://doi.org/10.1016/j.isci.2020.101688>



copy number) and energy (ATP) advantages compared to a digital approach for many biological functions that are low precision by nature. For example, we showed in a previous paper (Sarpeshkar, 2014) that the number of molecules needed to perform 2-bit precise addition is 3 orders of magnitude lower with an analog approach compared to a digital approach. The energy advantage of the same addition is almost 4 orders of magnitude lower when using an analog approach. By adopting an analog electronic circuit framework, we can use a language that describes biological processes more naturally. We also gain an appreciation for the power, speed, and precision trade-offs exhibited by nature when she makes complex circuits and systems function under tight resource constraints of power (ATP/sec) for a given speed (1/(time taken to do the computation)) and precision (signal-to-noise ratio or bits of precision) (Sarpeshkar, 2014).

All of the problems that we have described with respect to biological circuits and systems are also exhibited in analog electronic circuits, especially in those that have resource limitations with respect to energy and power and part count. For example, analog circuit designers also need to build robust functional devices using components that are often noisy at low electron copy number and that can be subject to significant manufacturing variations. Even well-characterized components sometimes exhibit unintended behaviors when operating in the context of a larger circuit due to loading, cross-talk, and feedback. Analog circuit designers often build systems that operate within a range of robustness and performance specifications while subject to constraints of power or physical space on an integrated circuit (chip) or board. For example, medical implants that are both small and power efficient (Bradley, 2006; Sarpeshkar, 2010) use ultra-low-power electronics to operate. Such electronic design is often made possible by a deep understanding of feedback systems that circuit designers have developed and refined over the past 100 years (Sarpeshkar 2010, 2014) for linear and nonlinear circuits.

Given the many similarities between biological and electronic circuits, we posited in a previous review paper that 17 synthetic biological circuits over 20+ years could be effectively studied through the lens of analog circuits for obtaining insight into their operation at the DNA, RNA, protein, or small-molecule/metabolite levels (Teo et al., 2015). Figures S1 and S2 and associated captions summarize the key ideas in this paper for the reader's convenience. Intuitively, flow variables can be mapped to current; state variables can be mapped to voltage; relationships between these variables, whether linear or nonlinear, map to corresponding current-voltage relationships as in Figure 3. Readers interested in detailed mathematical derivations of biochemical reaction networks can also find them in chapter 24 of (Sarpeshkar 2010) with associated hardware work described in (Woo et al. 2015, 2018; Kim et al., 2018). Important relationships between energy, information, and power in cells can be found in (Sarpeshkar 2014). Here, we suggest a four-pronged interdisciplinary methodology that is capable of leveraging the full power of analog electronic circuit design for general modeling, design, analysis, rapid simulation, and electronic reporting and measurement of biological circuits as shown in Figure 1. The Results subsections of our paper are organized as follows. In Section I, we discuss how to create electronic circuit schematics that are an exact representation of mathematical equations that describe biological circuits and use the enzyme-substrate binding circuit as an example (Figures 2 and 3). In Section II, we show how existing electronic circuit software, e.g. Cadence, which has been used for the hierarchical design of billions of electronic transistor devices on modern complex integrated circuit chips for decades, can be leveraged for the design of biological circuits. To show how our method can work in concrete detail and practice, we focus on a synthetic microbial biological operational amplifier circuit as shown in Figure 4. In Section III, we discuss how custom cytomorphic integrated circuit chips can rapidly simulate many instantiations and parameters of biological circuits that have been compiled into equivalent electronic circuits and thus help with automated parameter discovery and automated data fitting of measured biological data. We show a concrete example w.r.t. to the synthetic biological operational amplifier (Figures 5, 6, and 7). In Section IV, we illustrate how bio-electronic rather than bio-optical reporting and measurement can further help with the merging of biology and electronics with respect to such automation (Figure 8). We conclude by discussing the potential impact of our work in the future. Supplemental Sections I-III provide further details that correspond to Sections II and III in the main body of the paper.

Section I: Mapping Bio-Molecular Interactions to Electronic Circuits

Bio-molecular interactions are generally represented by cartoon illustrations and modeled by systems of ordinary differential equations (ODEs). Cartoons are great for developing intuition of simple biological systems but are often too coarse and abstract for developing deep insights. On the other hand, ODE models provide detailed mathematical descriptions of the dynamics of bio-molecular interactions; however, as

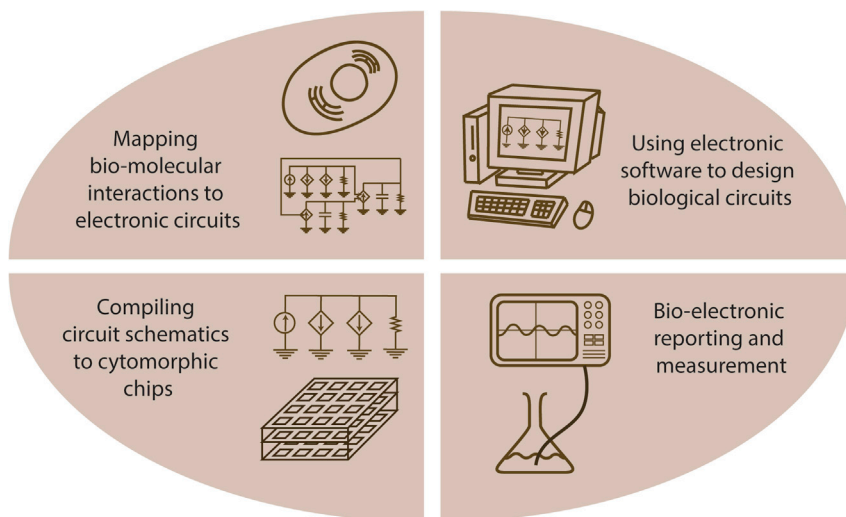


Figure 1. A Framework for Merging Biological and Electronic Circuits

The framework consists of four parts – (1) Biological circuits are represented as pictorial analog electronic circuit schematics that represent their mathematical dynamics exactly and quantitatively while preserving intuition about several circuit aspects such as feedback loops; (2) Electronic circuit software is then used for rigorous design, analysis, and simulation of these schematics; (3) The electronic circuit schematics are then compiled to and simulated on digitally programmable analog “cytomorphic” chips for rapid parameter discovery, automation, and learning including highly computationally intensive stochastic dynamics; (4) Further automation can be achieved if bioelectronic reporting and measurement is also electronic rather than optical such that the feedback loops between design, modeling, analysis, simulation, parameter discovery, fitting of data, and learning are completely electronic.

system complexity scales, they are difficult to interpret meaningfully. We have developed a mapping from biology to electronics that combines the ease of interpretation of illustrations with the mathematical exactness of ODEs. It can be applied to all circuits in molecular biology at the DNA, RNA, protein, and small-molecule levels, which we have illustrated as a canonical circuit schematic in a previous review (Teo et al., 2015) and in Figure S2. To demonstrate how the general mapping works, outlined in Figure 3, we use the specific and ubiquitous example of an enzyme-substrate (ES) binding reaction shown in Figure 2.

ES binding is typically represented by a cartoon or a mass action equation as in Figure 2. The cartoon provides a quick visual description while the equations capture the underlying thermodynamics. The equations in Figure 2 show that the rate of association of E and S depends on the product of free enzyme and free substrate multiplied by a forward rate constant K_f , while the rate of dissociation depends on the concentration of bound complex with a reverse rate constant K_r . We can represent such dynamics using a circuit where a current generator, resistor, and capacitor are connected in parallel. Such a pictorial circuit representation allows biological circuit designers to identify key characteristics such as feedback and noise without performing laborious calculations: Current fluxes through the current generator and resistor represent the association and dissociation molecular fluxes, respectively. As current flows in and out of the capacitor, its voltage changes accordingly. The voltage across the capacitor in this case corresponds to the concentration of bound substrate complex. The circuit subtracts bound variables from total conserved molecular variables to create free voltage variables via the voltage subtractors, creating two parallel “use-and-lose-it” negative feedback loops that are ubiquitously present in all chemical reactions. These “free voltage variables” are multiplied to generate a current that matches the forward association flux. The overall analog schematic is one that represents biological interactions succinctly while being faithful to the underlying mathematical descriptions including noise, dynamics, robustness, and feedback (Sarpeshkar, 2010, 2014; Teo et al., 2015). Figure S1, adapted from (Teo et al., 2015), provides further details.

Figure S1 shows that even diffusion can be exactly modeled via distributed resistor-capacitor (RC) circuits. Chapter 14 in (Sarpeshkar 2010) discusses how current-mode diffusor circuits can map such distributed RC circuits to highly efficient current-mode equivalents suitable for integrated circuit implementation, e.g., on the cytomorphic chips, discussed in Section III. In practice, as shown in Figure S5 and (Woo et al. 2015, 2018), cytomorphic chips and boards are assembled with field programmable gate arrays (FPGAs) for

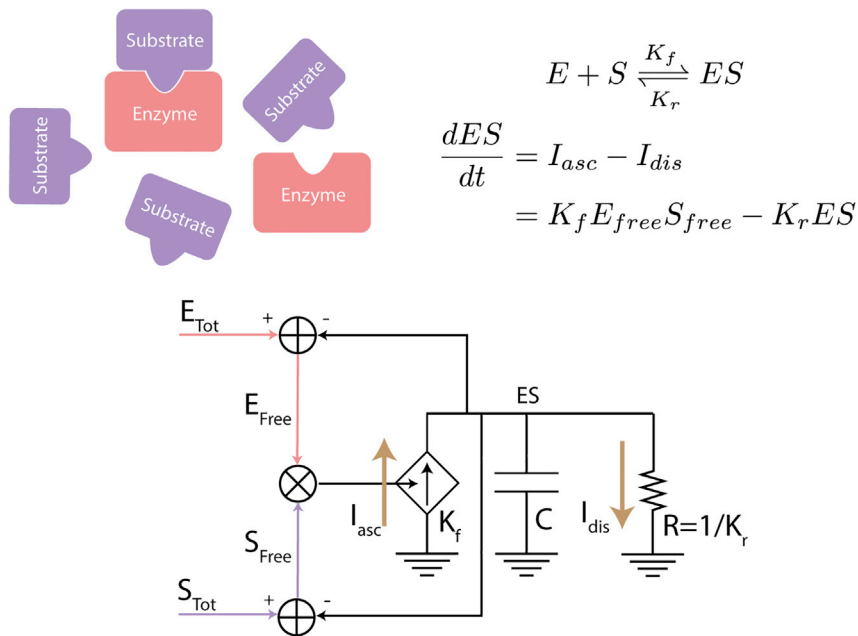


Figure 2. Enzyme-Substrate Binding as an Analog Circuit Schematic

The enzyme-substrate binding reaction is commonly represented by a chemical equation or cartoon blocks. The rate of complex association and dissociation is written in the form of coupled ordinary differential equations (ODEs). Using mappings described in the text and illustrated in Figure 3, we construct an analog circuit equivalent of an ES binding reaction. The latter circuit represents the mathematical dynamics of the ODE exactly while providing pictorial intuition on substrate depletion loading effects in chemical reactions, the stochastics of Poisson noise in the electronic current fluxes, and multiplicative and saturation non-linearities that are present in the reaction. Thus, it is very useful for design, modeling, analysis, and simulation of complex biological systems that can be composed in a hierarchical fashion out of such circuit schematics via software.

digital programmability of network connectivity and analog parameters. Therefore, via simple attenuation and delays in digital data packets to adjacent addresses, delays and diffusion can also be easily implemented in the digital domain.

To uncover properties of a biological circuit, we can study its analog schematic equivalent using analytical tools from analog circuit design. In the case of an ES binding circuit, the Poisson noise in ES flux is effectively the sum of Poisson noise from forward and reverse current fluxes in the dependent current generator and resistor, respectively, and determines the voltage or concentration noise on the capacitor (Sarpeshkar 2010, 2014). If the substrate negative feedback loop is effectively absent due to a large concentration of substrate, the enzyme negative feedback loop with a small-signal loop gain of $K_f S_{TOT}/K_r = S/K_D$ determines the proportional tracking of ES (output) with E_{TOT} (input) as in a simple negative feedback buffer operational amplifier circuit in electronics, generating well-known Michaelis-Menten input-output relationships. Figure 3 summarizes how mappings can be similarly created for 10 other common bio-molecular processes. The papers (Sarpeshkar, 2014; Teo et al., 2015) provide further details on the same treatment for several other well-known circuits from synthetic biology.

Section II: Using Electronic Circuit Software for Biological Circuit Design

Circuits, which convert equations to pictures, enable a big picture intuitive view of a whole system with all of the important feedback loops and interactions visibly obvious in a schematic or map. It is possible to design small circuits without such a schematic by using only mathematical equations. But, for design, analysis, and simulation of circuits and systems with hundreds to millions of state variables, pictorial intuition, model-order reduction, and hierarchy are essential. It is also important that we have the ability to rapidly switch the complexity of a model in a simulation to see if it actually matters at the timescale and for input-output relationships that are of relevant experimental biological importance in a practical application. For example, a “level 1” model with two experimentally constrained parameters may be more useful in a practical


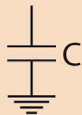
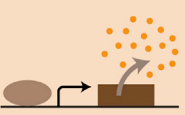



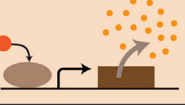



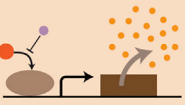
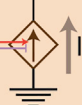
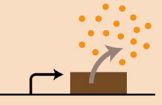

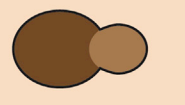
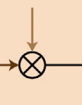
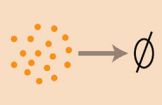
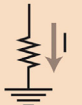


Cell Volume			Unregulated Constitutive Flux		
		A capacitor 'stores' molecular number and concentration state just like a cell itself does.			An independent (circular) current source represents constitutive molecular production.
Molecular Number			Regulated or Controlled Flux		
		Charges stored in the capacitor represents the molecular number in a cell.			A dependent (diamond) current source represents regulated production with a control or regulating input arrow coming into it.
Molecular Concentration			Multiple Controlling Inputs		
		Voltage represents the molecular concentration of RNA, Protein, DNA, or other small-molecule concentration			A diamond current source with multiple input arrows coming into it represents regulation by multiple molecules.
Molecular Flux			Binding of Two Molecules		
		Current flowing into the circuit represents an increase in target molecule, typically via production.			A voltage multiplier represents the binding of two molecules.
Degradation Flux			The Concentration of Free or Bound Variables		
		Current flowing out of the circuit represents a loss of target molecule typically via degradation.			A voltage adder is used to calculate free variable concentration by subtracting bound from total variable.

Figure 3. Mapping of Biological Circuits to Electronic Circuits

The table illustrates how mappings of biological concentration variables, represented as voltage, and biological flux variables, represented as current, are used to create controlled (dependent) and constitutive (independent) current sources and other electronic circuit equivalents. Such electronic circuit equivalents of biological circuits represent their operation faithfully including noise, nonlinearity, dynamics, and loading effects.

application even though the actual biology may involve significantly more parameters in an accurate "level 57" model with 1,000s of free parameters, many of which are unknown and are not experimentally constrained or relevant. Thus, certain subsystems can be well approximated with reduced-order input-output circuits: Finally, analog schematics are important for the scaling of biological circuits from simple low-level circuit motifs to circuits that can be connected and composed to create large-scale systems that are composed in a hierarchical fashion: For example, many ES reactions in cascade can form a glycolysis circuit, which itself can be a sub-circuit in a higher level glucose-to-ATP circuit. The glucose-to-ATP circuit can be a metabolic driving circuit with an effective nonlinear driving source impedance that powers other small and large subsystems within a cell. Many such subsystems can form the system of the cell.

Hierarchical and complex circuit design can be ported from electronic to biological circuit design with existing software. Over about 50 + years, analog circuit designers have developed computer-aided design software such as Cadence and circuit simulation tools such as SPICE to visualize circuits and to simulate them with ease (see Figure S3). SPICE also comes packaged with over 25 analysis tools, e.g. to perform small-signal .AC frequency analysis; to study transient .tran time-domain behavior; to study steady-state .DC input-output behavior; to see the effects of noise via .PNOISE; or to use monte-carlo simulation to study parameter sensitivity. Such tools can be leveraged rather than re-inventing the wheel from scratch. Schematic circuits at one level of a hierarchy can be connected to create a higher-level input-output circuit at the next level of hierarchy, which is represented abstractly by a circuit "symbol". Such symbols can then be combined with each other to create higher level circuits. The process can be recursively repeated to create systems of massive complexity. The microprocessor and analog cell phone chips that we take for granted today, which often have billions of interconnected transistor devices, were designed in such a

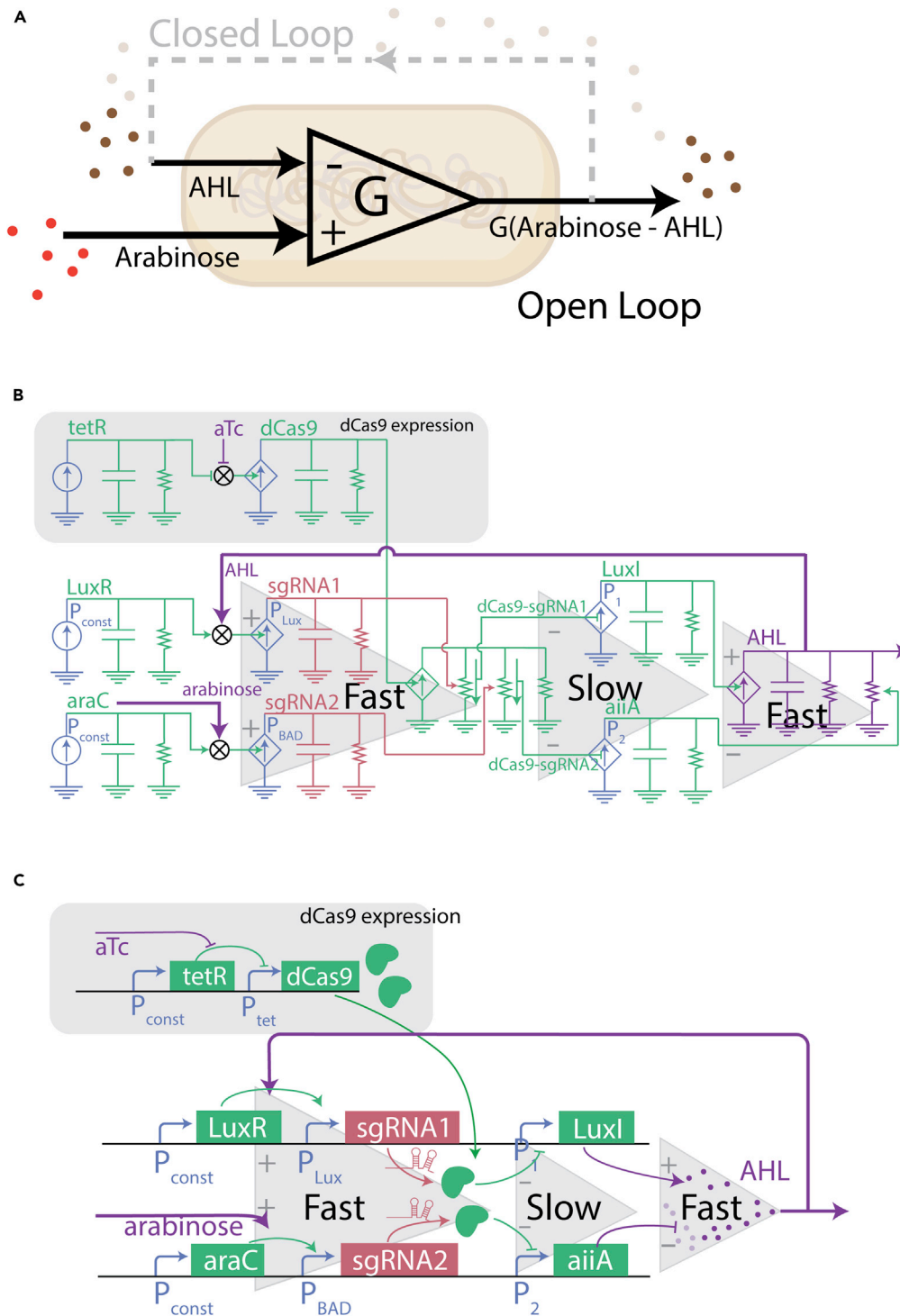


Figure 4. Biological Operational Amplifier

(A) In open-loop configuration, the biological operational amplifier amplifies the difference between two input concentrations of small molecules such as AHL and arabinose to create a large concentration of an output target biomolecule. When the output biomolecule is the same as the input at the negative terminal, a negative feedback loop enhances robustness to parameters, buffering, and tracking performance can be achieved.

(B) The biological operational amplifier (Bio-OpAmp) has three amplification stages. The first stage is a fast stage that generates guide RNAs based on the input concentration of AHL and arabinose. The sgRNAs bind to CRISPR dCas9, and

Figure 4. Continued

the resulting complex inhibits either LuxI or AiiA expression in the second stage. The concentration of aTc regulates dCas9 expression, which enables control of the total strength of the inhibition. The last amplification stage is a fast stage that uses LuxI and AiiA to synthesize or degrade AHL, respectively. AHL binds to LuxR at the inverting input to close the feedback loop.

(C) To represent the production of bio-molecules in its stages of amplification, the schematic uses a circuit motif similar to the enzyme-substrate binding motif in [Figure 2](#).

fashion. Here, we shall only provide an example of a relatively simple synthetic biological operational amplifier circuit to illustrate how electronic circuit software can be concretely used for creating biological circuit schematics. Nevertheless, it will illustrate all of the concepts. Subsequently, we shall focus on discussing how to compile, simulate, discover parameters, and fit data in an automated fashion.

Synthetic biologists have designed and ported many basic electronic circuit motifs such as logic gates ([Bonnet et al., 2013](#); [Maung and Smolke, 2008](#); [Nielsen et al., 2016](#)), latches ([Gardner et al., 2000](#); [Lee et al., 2016](#)), load driver circuits ([Mishra et al., 2014](#)), oscillators ([Chen et al., 2015](#); [Elowitz and Leibler, 2000](#); [Prindle et al., 2014](#)), and log-linear circuits ([Daniel et al., 2013](#)) to biology. In contrast, the operational amplifier (OpAmp), which is a popular device used in analog circuits, has only just started gaining traction ([Klavins, 2014](#)). An OpAmp is often considered a fundamental building block for designing large regulatory loops in analog circuits due to its many attributes for modulating feedback robustly. It implements a simple circuit building block wherein the voltage difference of its two control inputs is amplified with a large gain and reported at its output terminal (see [Figure 4](#) and Appendices from [Zeng et al., 2018](#)). When connected to companion components in a negative feedback loop, an OpAmp enables robust and precise analog computations such as weighted summation, inverting and non-inverting amplification, and integration. It performs these calculations rigorously despite being susceptible to manufacturing variations. An OpAmp's robustness to parameter variation is essential for making analog electronics that are scalable, versatile, and context independent from an input-output point of view. Therefore, by building a biological OpAmp (Bio-OpAmp) ([Zeng et al., 2018](#)), we can leverage its properties to regulate feedback in a variety of important biological processes such as homeostasis ([Berridge et al., 2003](#); [Nemazany et al., 2015](#); [Wong et al., 2012](#)), metabolic regulation ([Pan et al., 2009](#); [Sturm et al., 2010](#)), and immune response ([Fukao et al., 2002](#); [Liu et al., 2015](#)).

The Bio-OpAmp design shown in [Figures 4A–4C](#) is a concrete instantiation of the framework of [Figure 1](#). It is largely inspired by a classical three-stage operational amplifier ([Zeng et al., 2018](#)). An electronic OpAmp typically has three gain stages: an initial high-bandwidth input stage, an intermediate amplification stage, and a high-bandwidth output stage. The Bio-OpAmp mimics this architecture using a combination of transcription and translation regulatory mechanisms (See [Figure 4B](#)). The first stage is a fast differential input stage that senses the difference between arabinose (non-inverting signal) and acyl homoserine lactone (AHL) (inverting signal) and generates corresponding guide RNAs (sgRNAs). The sgRNAs compete for binding with dCas9, such that when sgRNA1 binds to dCas9, it removes a potential binding site for sgRNA2 and vice versa, thereby amplifying the input signal via a “push-and-pull” mechanism. The second stage is a slow differential stage that uses bound dCas9-sgRNA complexes to downregulate AiiA and LuxI protein expression levels. Since each mRNA transcript of AiiA and LuxI is translated to multiple copies of their respective proteins, changes to sgRNA levels are amplified via this downstream increase in copy number. Translation generally happens on a slower timescale than transcription, so the second stage is slower to respond to changes. The third stage is a fast differential stage where AiiA and LuxI enzymes degrade or produce AHL, respectively. Since each enzyme can potentially catalyze multiple copies of AHL, the third stage creates yet another level of amplification. Additionally, since both enzymes catalyze production/degradation of the small molecule, they effectively combine the two inputs into a single-ended output. When the three gain stages are combined, they produce a large open-loop gain that is difficult to achieve using only a single gain stage in isolation due to biological limitations.

Further details of the Bio-OpAmp w.r.t use of electronic circuit software for biological circuit design including robustness, sensitivity to parameters, buffering capability, oscillation, and tracking performance are described in [Supplemental Section I](#) of this paper. [Figures S10–S14](#) and [Figure 7](#) show several details of its performance, comparing circuit software and circuit hardware instantiation on cytomorphic chips. We shall now focus on an important part of the framework of [Figure 1](#), namely the compilation of circuit schematics to cytomorphic chips.

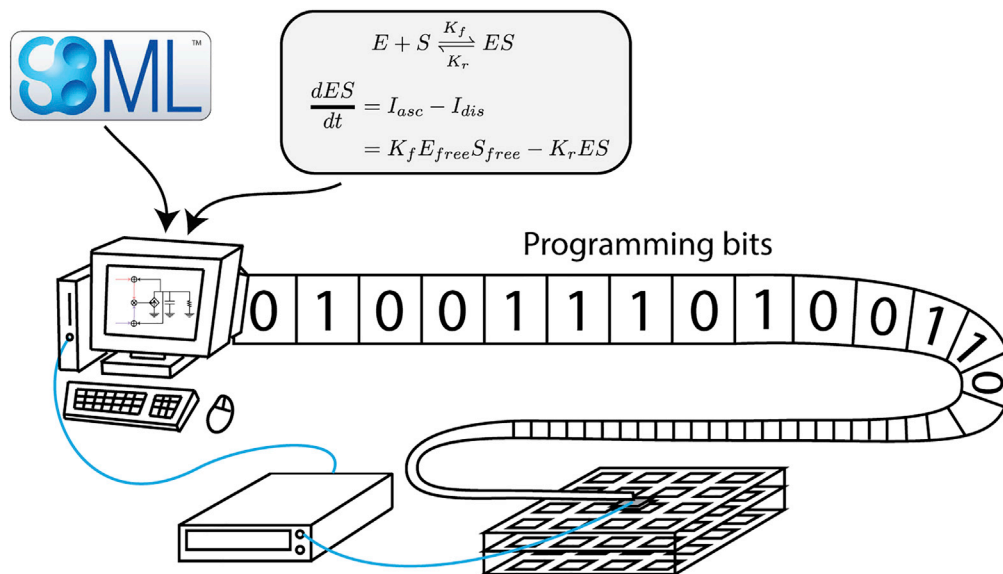


Figure 5. Computational Pipeline to Program Cytomorphic Chips and Systems for Automating Parameter Discovery and for Learning

Using compilers that have been developed or are currently in development (Medley et al., 2020), we translate biochemical reactions in SBML or in SPICE netlists to programming bits for the cytomorphic chips that have hardware instantiations of chemical reaction circuits. To aid in such programming, MATLAB and Simulink interfaces interact with field programmable gate arrays (FPGAs) on circuit boards composed of many such cytomorphic chips. The programmable bits configure DACs, switches, and bio-molecular network connectivity on the cytomorphic chips.

Section III: Compiling Circuit Schematics to Cytomorphic Chips for Fast Simulation, Parameter Discovery, and Data Fitting

While existing circuit software tools like Cadence are useful for the design of large-scale systems and the simulation of relatively small circuits like the Bio-OpAmp, the simulation of large-scale biological systems can be slow on general-purpose digital computers. In particular, stochastic stimulations of relatively low-copy-number molecular variables are slow even for systems with as few as 10 variables (Gibson and Bruck, 2000; Li and Petzold, 2010; Ramaswamy et al., 2009). Such simulations require Poisson process emulation via the Gillespie stochastic simulation algorithm (GSSA), which is extremely computationally intensive on digital computers, regardless of the software package used (MATLAB, Cadence, COPASI, ...) (Kim et al., 2018; Woo et al., 2015). They are not parallelizable due to the need to faithfully emulate asynchronous Poisson processes and create pseudo-random numbers at every time step on synchronous digital computers with fixed time steps and clocks. Stiff differential equations with diffusion and compartmentalization exacerbate such problems.

Fortunately, deterministic and stochastic simulations of large-scale bio-molecular dynamical systems can be done extremely quickly on digitally programmable highly parallel asynchronous analog cytomorphic systems (Sarpeshkar 2010; Kim et al., 2018; Woo et al., 2015, 2018). These systems have a flat simulation time even as reaction network size or the number of species scales. Some of these systems amplify natural thermal noise to achieve highly stochastic simulations or use inherent analog noise in current fluxes for moderate levels of noise (Kim et al., 2018). Their readouts and programmability are compatible with traditional digital computers such that the user can be agnostic to the details of internal chip operation, viewing such simulations as simply originating from a fast custom Bio co-processor. While there is an argument to be made for keeping model complexity low such that data can be interpreted more meaningfully, biology as a whole is moving toward understanding bigger and more complex systems. Knowledge of such systems is rapidly progressing because of advances in next-generation sequencing technology and because of the advent of big data and machine learning. Thus, it is advantageous to compile circuits to cytomorphic chips for fast simulation and then leverage cytomorphic chip simulations to train large biological networks that fit biological data. In this paper, we shall only briefly summarize how these cytomorphic chips operate. Readers interested in further details should consult past work over more than

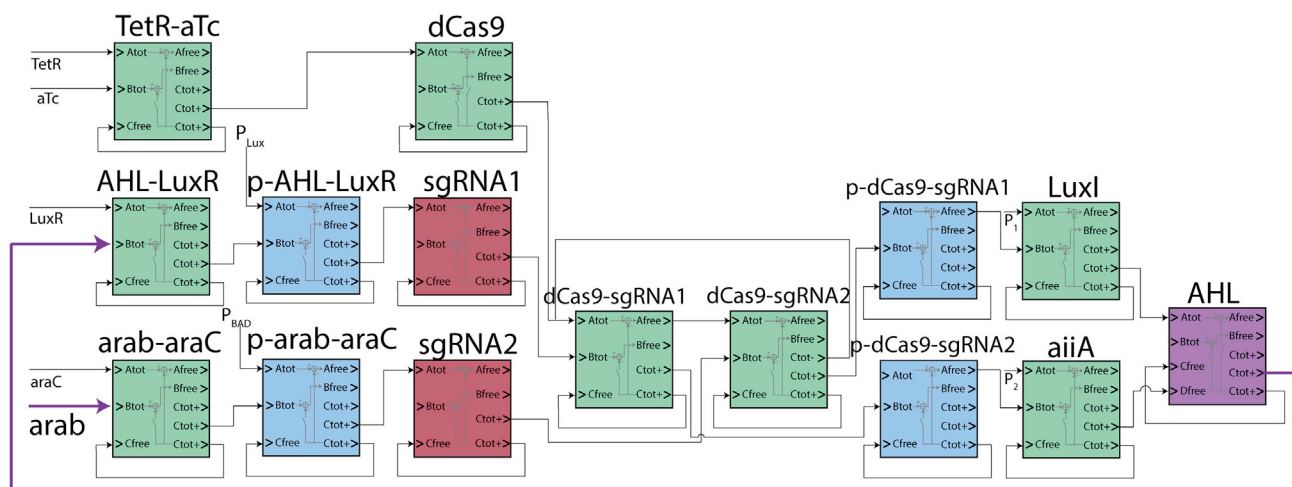


Figure 6. A Compilation of the Bio-OpAmp Circuit to an Equivalent Cytomorphic Chip Instantiation

Figures S6–S9 illustrate how to generate a cytomorphic configuration of the Bio-OpAmp in detail.

a decade (Sarpeshkar et al., 2005a; Mandal and Sarpeshkar, 2009a, 2009b; Sarpeshkar, 2010; Kim et al., 2018; Woo et al., 2015, 2018).

As described extensively in the latter papers, the same equations of Boltzmann exponential thermodynamics govern the stochastics of molecular reaction dynamics as well as current flow in subthreshold electronic transistor circuits. Thus, a mapping of the mathematical differential equations that govern interactions between molecules with log (molecular concentration) mapped to voltage and molecular flux mapped to current, respectively, lead to an efficient and exact translation of nonlinear biological circuits and systems to equivalent nonlinear electronic circuits and systems that simulate them. Such physical emulation to do fast simulation is analogous to the idea of using GHz inductor-capacitor-resistor (LCR) electronic circuits to simulate slow spring-mass-damping mechanical circuits. In the papers (Kim et al., 2018; Woo et al., 2015, 2018), the authors describe the architecture, specifications, and performance of the cytomorphic chips in detail. The authors demonstrate the ability of the chips to be digitally configured to simulate any biochemical reaction network using programmable circuit building blocks. For example, we can simulate synthesis, degradation, association, dissociation, dimerization, substitution, cascade, fan-in, fan-out, and loop networks by appropriately configuring and connecting analog circuit blocks. Figure S5 shows the key circuit building block, and Figures S6B and S6C provide specific examples of a branching network important for competitive drug binding and ES reactions, respectively. Other examples that have been described include the dynamics and stochastics of a repressor, a p53-MDM2 cancer pathway, and glycolytic oscillations. Even for modest networks with only about 80 stochastic reactions, cytomorphic simulations exhibit a significant 700X speedup over digital COPASI simulations or 30,000x speedup over digital MATLAB simulations, while yielding identical results (Woo et al., 2015, 2018). For large-scale systems, such speedups could be greater than a million fold (Woo, 2016).

Building on such prior work, we were motivated to compile and simulate the Bio-OpAmp with cytomorphic chips. To do so, we developed a mapping between analog circuit representations useful in this particular Bio-OpAmp case and circuits on cytomorphic chips. The Bio-OpAmp uses three primary motifs: a transcription-translation motif, a fan-out motif for substrate competition, and a dependent production and degradation motif for AHL regulation. Figures S7–S9 and Supplemental Sections I and II discuss these mappings in greater detail. The circuit in Figure 4C is compiled to its cytomorphic equivalent in Figure 6 using these mappings. Specifically, we use the translation-transcription cytomorphic block from Figure S7 in OpAmp gain stages 1 and 2; we use the conductance divider cytomorphic block that models sgRNA and dCas9 binding from Figure S8 in OpAmp gain stage 1; we use the AHL production-degradation cytomorphic block from Figure S9 in OpAmp gain stage 3.

The pipeline shown in Figure 5 enables us to program the chip and run multiple simulations of the Bio-OpAmp in parallel. The pipeline can be adapted to read SBML files using a compiler that was developed recently by Medley et al. (2020). It is worth noting that digital calibration can drastically improve the

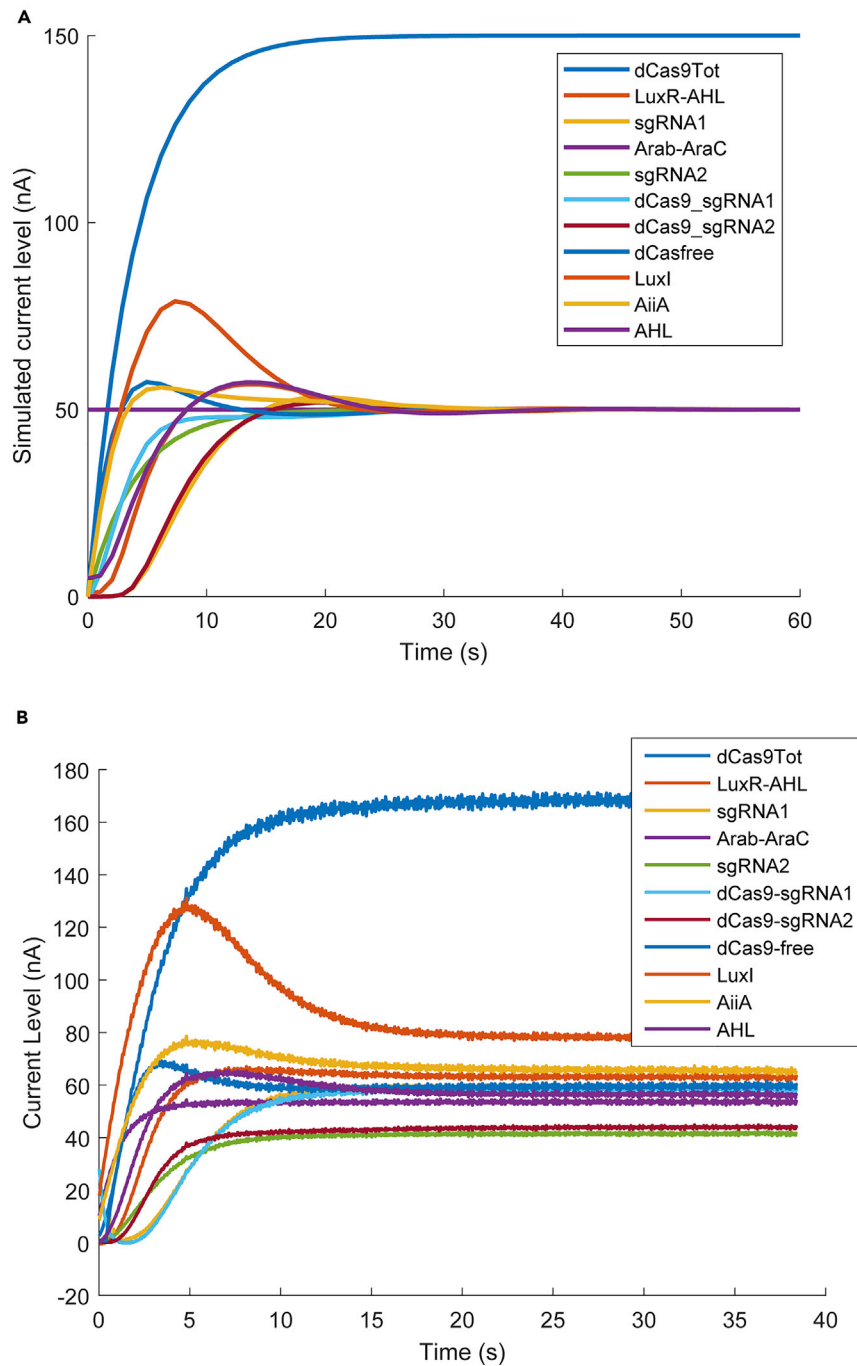


Figure 7. Dynamics of a Bio-OpAmp as it Reaches Equilibrium

(A) Software simulation data.

(B) Cytomorphonic chip simulation data. The time series illustrate the transient response of the Bio-OpAmp using normalized concentrations centered at 50 nA. Both simulations exhibit similar transient behavior including overshoots, rise time, and settling time. In the cytomorphonic simulation, current levels at equilibrium deviate from 50 nA due to manufacturing variability in the chips.

precision and variability of analog circuits (Sarpeshkar, 2010). Calibrating analog-to-digital converters (ADCs), digital-to-analog converters (DACs), and other analog circuits to yield high-precision, low variability analog systems has been proven in cochlear implants for deaf patients (Sarpeshkar et al, 2005a,

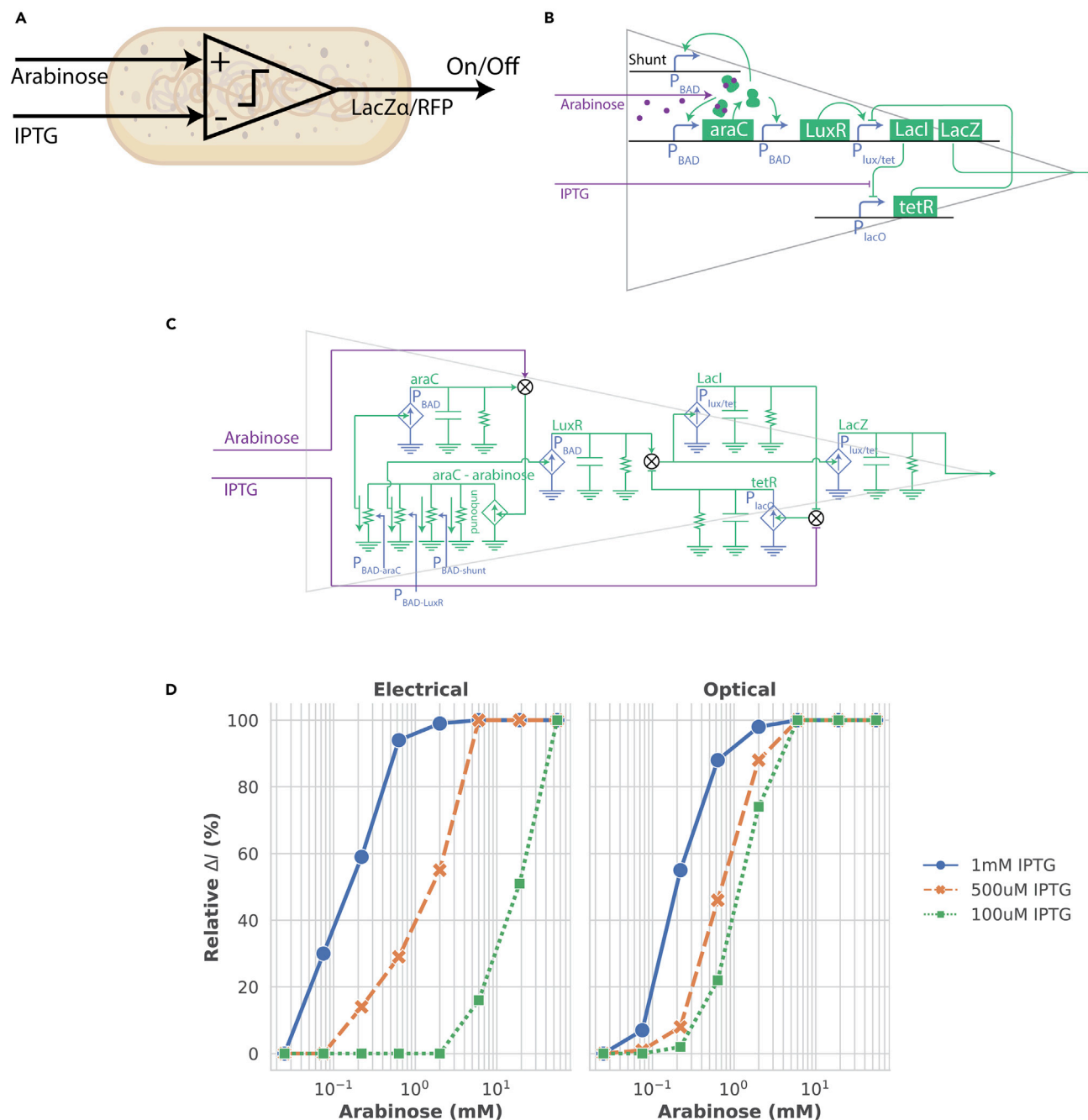


Figure 8. Biological Comparator

(A) Biological circuit cartoon representation.

(B) Transcription regulation network of biological comparator.

(C) Analog circuit schematic representation of biological comparator.

(D) Measured biological data comparing bio-electronic and optical reporting performance that is adapted from (Zeng et al., 2019).

2005b) and in other applications (Sarpeshkar, 2010). Such calibration would be needed in actual commercial or large-scale systems. However, they do not alter the conclusions of our smaller-scale proof-of-concept demonstrations here such that we shall not focus on them.

Figures 7A and 7B show that Cadence software simulations and cytomorphic chip simulations of the Bio-OpAmp are in good agreement, illustrating how the general framework of Figure 1 can be concretely

instantiated in practice. Using the pipeline of [Figure 5](#), we programmed multiple chips to simulate the Bio-OpAmp in parallel as shown in [Figure S10](#). Chip-to-chip variations in such simulations can be calibrated for digitally as in a past cochlear implant for the deaf, which worked on a deaf subject on the first try ([Sarpeshkar, 2010](#); [Sarpeshkar et al., 2005b](#)).

We simulated the Bio-OpAmp in electronic circuit software and on cytomorphic chips with varying concentrations of AHL and arabinose. These simulations replicate the biological experiments in ([Zeng et al., 2018](#)) that characterize the open- and closed-loop behavior of the Bio-OpAmp: As shown in [Figure S11](#), the steady-state AHL concentration (reported as RFP in the experiments) tracks input arabinose closely while rejecting the added disturbance input AHL in closed-loop configurations. In an open-loop configuration, output AHL exhibits non-linear input-output characteristics with input arabinose that are reminiscent of the saturation function used to describe cooperative binding. The steady-state outputs from biological data, software simulation, and cytomorphic chip implementation are in good agreement, suggesting that the schematic and cytomorphic circuit models of [Figures 4](#) and [6](#) are indeed accurate.

We ran high-throughput cytomorphic simulations to perform sensitivity analysis and parameter discovery to optimize the Bio-OpAmp. For example, the open-loop gain is maximized when the dissociation constants of sgRNA1 and sgRNA2 are similar, as shown in [Figure S12](#). This finding illustrates the importance of symmetry in all feedback systems and high-performance circuits. The closed-loop gain in [Figure S13](#) is also in accord with predictions of such gain from small-signal analysis corresponding to [Figure S4](#) or ([Zeng et al., 2018](#)). [Figure S14](#) shows that the steady-state tracking error is also in accord with the overall gain of the OpAmp as predicted from feedback system theory. Chapter 5 of ([Teo, 2019](#)) provides a more detailed discussion including additional findings based on parameter discovery and machine learning. A short conference paper ([Teo et al., 2019](#)) presents a highly abbreviated version of some portions of this journal paper.

In biological systems, due to low molecular copy numbers and/or high burst noise factor, the dominant measured noise is of thermal origin, has a flat or “white” power spectral density, and obeys the Poisson statistics of uncorrelated current flow at the fundamental chemical reaction level (Chapter 7 on noise in [Sarpeshkar 2010](#); [Sarpeshkar 2014](#)). Hence, as in the GSSA, we have mostly focused on only discussing the emulation of such Poisson noise, which is fundamental to all thermodynamic processes. However, at the system level, due to correlations, explicit feedback, filtering, self-organization, scale invariance, and “defects” in biological membranes and other biological structures, one can also see “pink noise” with a sloping power spectrum at frequencies below a certain relatively low corner frequency. Such noise is observed in electronic transistors as well due to “traps” or “mobility fluctuations” in current flow where it is often called “1/f noise” or “power-law noise”. From quantitative models of such power-law noise in devices and circuits as discussed in chapters 7, 8, 12, 13, 14, and 24 in ([Sarpeshkar 2010](#)), we can certainly also emulate such biological noise both explicitly, e.g., as the noise in the membrane, and implicitly, e.g., if it emerges in circuits due to time-scale invariance in certain systems, e.g. heartbeats and traps in transistors. Such emulations can be done in both circuit software and cytomorphic chip hardware if desired. In fact, most electronic circuit software has such 1/f noise models by default to ensure that electronic circuits perform as desired.

As discussed in chapter 19 in ([Sarpeshkar 2010](#)), emergent properties such as “stochastic resonance” wherein the detectability of a signal is improved if an optimal amount of noise helps it cross a fixed threshold can emerge in both electronics and biology and can also be easily represented and modeled. Such effects may be present in p53 in cancer networks, among the networks that we have been able to successfully model. In fact, we can even quantitatively model fundamental and system noise in any circuit including the Bio-OpAmp. However, as in several synthetic biological circuits to date, the Bio-OpAmp is implemented with relatively high copy numbers of molecules with many cells in solution. Thus, Bio-OpAmp open-loop gains were nearly always stably measured to be in the 50–100 range, both in experimental biological measurements and in quantitatively accurate models that fit such biological data ([Zeng et al., 2018](#)). While current optical reporting and measuring systems in biology, which are not prohibitively expensive, cannot easily and non-destructively measure signal and noise in a single cell easily, the more sensitive bio-electronic systems, which we describe in Section IV, may be capable of such measurements in the future. Hence, we shall discuss them now.

Section IV: Bio-Electronic Reporting and Measurement.

New synthetic regulatory network designs are increasingly driven by iterative design-built-test-learn (DBTL) cycles ([Carbonell et al., 2018](#); [Opgenorth et al., 2019](#)). While the field has developed many logic-based tools

to accelerate and simplify the circuit prototyping process, the testing and validation process is still based on making optical measurements of a fluorescent or luminescent reporter molecule produced by the circuit. Many modern methods such as fluorescent microscopy, flow cytometry, and short-read sequencing make use of fluorescent proteins for their core functions (Bentley et al., 2008; Lichtman and Conchello, 2005; Lyons and Parish, 1994). Optical biosensors are used in many canonical circuits in synthetic biology (Elowitz and Leibler, 2000; Stricker et al., 2008), and they continue to be the default mode of reporting in most biological circuits. However, despite their popularity, optical biosensors present several caveats; fluorescent proteins cause cytotoxicity when produced in large concentration (Shen et al., 2017); fluorophores undergo photobleaching when exposed to long periods of excitation (Greenbaum et al., 2000) reducing dynamic range and limiting the number of consecutive measurements; long photoexcitation causes phototoxicity by generating reactive oxygen species that damage the cell (Ganini et al., 2017). Due to these limitations, fluorescent biosensors are unsuitable for reporting certain types of behavior such as taking continuous readings in time-lapse microscopy, which may be necessary for a DBTL paradigm.

To create biosensors for a wider range of circuits, we need biosensors that can take real-time measurements, have a wide dynamic range and good sensitivity, and do not cause significant cell death. As an example, we developed a microbial fuel cell (MFC) that uses an electricigenic bacterium to generate currents based on circuit activity (Zeng et al., 2019). The fuel cell consists of a co-culture of *E. coli* MG1655 and *S. oneidensis* MR-1 that resides on the anode. A co-culture system was chosen because it exhibits greater tolerance to metabolic burden and cytotoxicity and experiences less cross-talk compared to monoculture systems (Lisa et al., 2014; Stephens et al., 2019). *E. coli* converts lactose in its environment to lactate with the aid of an intermediate reporting enzyme LacZ α while *S. oneidensis* metabolizes the resulting lactate and transfers the electrons to the anode using either direct electron transfer or metabolite (e.g. flavin)-mediated electron transfer (Busalmen et al., 2008; Okamoto et al., 2013, 2014). When we measure current in the MFC, we are effectively measuring the concentration of LacZ α in *E. coli*. To use the MFC as an electrical biosensor, we simply replace fluorescent protein genes on the plasmid with LacZ α and measure electrical current instead of fluorescence intensity.

As an example of how bio-electronic reporting can be instantiated in practice, a component of the framework of Figure 1, we compared the response of a biological comparator (Figure 8) using either a fluorescent reporter or our electrical reporter. An electronic comparator is a device that compares two inputs to generate an irreversible on/off output signal depending on whether one input is higher than the other. The biological comparator reproduces the same behavior by utilizing a wide dynamic range log-linear input analog LuxR circuit first described in (Daniel et al., 2013) and a subsequent positive feedback latch circuit as shown in Figure 8B. The LuxR circuit combines an analog positive feedback loop circuit and a decoy “shunt” circuit to increase the log-linear dynamic range with respect to the input Arabinose.

To generate an irreversible digital output, the comparator of Figure 8 uses LacI to repress TetR and vice versa, thereby creating a switch-like behavior. Arabinose activates LacI expression via LuxR while an inducer with action similar to lactose (IPTG) represses LacI activity. The relative strength of the two antagonistic effects decides the final reporter output. When using a fluorescent reporter (RFP), changes to IPTG concentration did not significantly affect the threshold concentration of arabinose required to switch the comparator on. In contrast, when using a LacZ α reporter, a higher IPTG concentration increases the threshold concentration of arabinose needed to flip the comparator (See (Zeng et al., 2019)). The wider dynamic range can be explained by LacZ α catalyzing lactose to lactate, which serves as a mode of signal amplification, improving both the measurement as well as providing a convenient electronic output.

CONCLUDING REMARKS

We have suggested how electronic circuit design and measurement can serve to automate design, modeling, analysis, simulation, and quantitative fitting of measured data as shown in the framework of Figure 1. We have also shown how such a framework can be concretely instantiated in a synthetic biological operational amplifier circuit in living microbial cells. While this work is in a proof-of-concept and foundational stage, in the future, large-scale biological circuits and systems for drug cocktail discovery could be designed and simulated quickly for a systems biology and medical application. Alternatively, precise and robust synthetic circuits for medicine, e.g. Bio-OpAmp-like homeostasis circuits for drug dosage control can benefit from the robust and predictive power of design automation, enabling quick applications in

multiple contexts rather than via tedious time-consuming experimentation. In both cases, the merging and unification of biology and electronics via unifying and hierarchical circuit motifs, accurate modeling and compilation, fast simulation for parameter discovery and learning, and bio-electronic measurement may help scale the design and understanding of biological systems. Thus, the current state, which is to do relatively simple or empirical design, could grow toward more complex and more rational design, which is highly important if medicine and bioengineering are to scale.

Limitations of the Study

We acknowledge that complex biological systems often require many unknown parameters to model, which is still an issue for us as well as for others. However, the combination of fast simulation such that a brute-force exploration of many parameters is possible via cytomorphic chips; of machine learning and data fitting associated with such exploration; the collapsing of many parameters and topologies into model-order-reduced input-output circuit equivalents and/or circuits with net feedback loop gains or gains that are dependent on the products of many parameters rather than on each as in our Bio-OpAmp; and the use of physical constraints such as energy, power, copy numbers, max. flux rates, flux balance, which are all very natural and easy and automatically entangled in circuits (Sarpeshkar, 2010, 2014) serve to make this problem not seem as daunting as it may seem. We hope that our four-pronged approach will help in this regard.

METHODS

All methods can be found in the accompanying [Transparent Methods supplemental file](#).

SUPPLEMENTAL INFORMATION

Supplemental Information can be found online at <https://doi.org/10.1016/j.isci.2020.101688>.

ACKNOWLEDGMENTS

We acknowledge useful discussions with Ji Zeng, Jaewook Kim, and Sung Sik Woo. This work was supported by the AFOSR under grant number FA9550-18-1-0467 and by the NIH under grant number R01 GM 123032-01 to R.S. J.T. was supported in part by funds from the A*STAR and by funds from Dartmouth College.

AUTHOR CONTRIBUTIONS

J.T. and R.S. designed the model and the computational framework. J.T. carried out the implementation and analyzed the data. J.T. and R.S. contributed to the writing of the manuscript. R.S. was in charge of overall direction and planning of the project.

REFERENCES

- Ausländer, D., Ausländer, S., Pierrat, X., Hellmann, L., Rachid, L., and Fussenegger, M. (2018). Programmable full-adder computations in communicating three-dimensional cell cultures. *Nat. Methods* 15, 57–60.
- Bentley, D.R., Balasubramanian, S., Swerdlow, H.P., Smith, G.P., Milton, J., Brown, C.G., Hall, K.P., Evers, D.J., Barnes, C.L., Bignell, H.R., et al. (2008). Accurate whole human genome sequencing using reversible terminator chemistry. *Nature* 456, 53–59.
- Berridge, M.J., Bootman, M.D., and Roderick, H.L. (2003). Calcium signalling: dynamics, homeostasis and remodelling. *Nat. Rev. Mol. Cell Biol.* 4, 517–529.
- Bonnet, J., Yin, P., Ortiz, M.E., Subsoontorn, P., and Endy, D. (2013). Amplifying genetic logic gates. *Science* 340, 599–603.
- Bradley, P.D. (2006). An ultra low power, high performance Medical Implant Communication System (MICS) transceiver for implantable devices. *IEEE 2006 Biomed. Circuits Syst. Conf. Healthc. Technol. Biocas 2006*, 158–161.
- Busalmen, J.P., Esteve-Núñez, A., Berná, A., and Feliu, J.M. (2008). C-type cytochromes wire electricity-producing bacteria to electrodes. *Angew. Chem. Int. Ed.* 47, 4874–4877.
- Carbonell, P., Jervis, A.J., Robinson, C.J., Yan, C., Dunstan, M., Swainston, N., Vinaixa, M., Hollywood, K.A., Currin, A., Rattray, N.J.W., et al. (2018). An automated Design-Build-Test-Learn pipeline for enhanced microbial production of fine chemicals. *Commun. Biol.* 1, 1–10.
- Cardinale, S., and Arkin, A.P. (2012). Contextualizing context for synthetic biology - identifying causes of failure of synthetic biological systems. *Biotechnol. J.* 7, 856–866.
- Chen, Y., Kim, J.K., Hirling, A.J., Josić, K., and Bennett, M.R. (2015). Emergent genetic oscillations in a synthetic microbial consortium. *Science* 349, 986–989.
- Daniel, R., Rubens, J.R., Sarpeshkar, R., and Lu, T.K. (2013). Synthetic analog computation in living cells. *Nature* 497, 619–623.
- Elowitz, M.B., and Leibler, S. (2000). A synthetic oscillatory network of transcriptional regulators. *Nature* 403, 335–338.
- Ferrell, J.E. (2002). Self-perpetuating states in signal transduction: positive feedback, double-negative feedback and bistability. *Curr. Opin. Cell Biol.* 14, 140–148.
- Fukao, T., Tanabe, M., Terauchi, Y., Ota, T., Matsuda, S., Asano, T., Kadowaki, T., Takeuchi, T., and Koyasu, S. (2002). P13K-mediated negative feedback regulation of IL-12 production in DCs. *Nat. Immunol.* 3, 875–881.
- Ganini, D., Leinisch, F., Kumar, A., Jiang, J.J., Tokar, E.J., Malone, C.C., Petrovich, R.M., and Mason, R.P. (2017). Fluorescent proteins such as eGFP lead to catalytic oxidative stress in cells. *Redox Biol.* 12, 462–468.

- Gardner, T.S., Cantor, C.R., and Collins, J.J. (2000). Construction of a genetic toggle switch in *Escherichia coli*. *Nature* 403, 339–342.
- Gibson, M.A., and Bruck, J. (2000). Efficient exact stochastic simulation of chemical systems with many species and many channels. *J. Phys. Chem. A* 104, 1876–1889.
- Greenbaum, L., Rothmann, C., Lavie, R., and Malik, Z. (2000). Green fluorescent protein photobleaching: a model for protein damage by endogenous and exogenous singlet oxygen. *Biol. Chem.* 381, 1251–1258.
- Kim, J., Woo, S.S., and Sarpeshkar, R. (2018). Fast and precise emulation of stochastic biochemical reaction networks with amplified thermal noise in silicon chips. *IEEE Trans. Biomed. Circuits Syst.* 12, 379–389.
- Klavins, E. (2014). Lightening the load in synthetic biology. *Nat. Biotechnol.* 32, 1198–1200.
- Lee, J.W., Gyorgy, A., Cameron, D.E., Pyenson, N., Choi, K.R., Way, J.C., Silver, P.A., Del Vecchio, D., and Collins, J.J. (2016). Creating single-copy genetic circuits. *Mol. Cell* 63, 329–336.
- Li, H., and Petzold, L. (2010). Efficient parallelization of the stochastic simulation algorithm for chemically reacting systems on the graphics processing unit. *Int. J. High Perform. Comput. Appl.* 24, 107–116.
- Lichtman, J.W., and Conchello, J.A. (2005). Fluorescence microscopy. *Nat. Methods* 2, 910–919.
- Lisa, G., Paul, F., and Polizzi, K.M. (2014). Co-culture systems and technologies: taking synthetic biology to the next level. *J. R. Soc. Interfaces* 11, 20140065.
- Liu, Z., Gerner, M.Y., Van Panhuys, N., Levine, A.G., Rudensky, A.Y., and Germain, R.N. (2015). Immune homeostasis enforced by co-localized effector and regulatory T cells. *Nature* 528, 225–230.
- Lyons, A.B., and Parish, C.R. (1994). Determination of lymphocyte division by flow cytometry. *J. Immunol. Methods* 171, 131–137.
- Zeng, J., Teo, J.J.Y., Banerjee, A., Chapman, T.W., Kim, J., and Sarpeshkar, R. (2018). A synthetic microbial operational amplifier. *ACS Synth. Biol.* 7, 2007–2013.
- Mandal, S., and Sarpeshkar, R. (2009a). Log-domain circuit models of chemical reactions. In *2009 IEEE International Symposium on Circuits and Systems*, (IEEE), pp. 2697–2700.
- Mandal, S., and Sarpeshkar, R. (2009b). Circuit models of stochastic genetic networks. In *2009 IEEE Biomedical Circuits and Systems Conference*, (IEEE), pp. 109–112.
- Maung, N.W., and Smolke, C.D. (2008). Higher-order cellular information processing with synthetic RNA devices. *Science* 322, 456–460.
- Medley, J.K., Teo, J., Woo, S.S., Hellerstein, J., Sarpeshkar, R., and Sauro, H.M. (2020). A compiler for biological networks on silicon chips. *PLoS Comput. Biol.* 16, e1008063.
- Mishra, D., Rivera, P.M., Lin, A., Del Vecchio, D., and Weiss, R. (2014). A load driver device for engineering modularity in biological networks. *Nat. Biotechnol.* 32, 1268–1275.
- Mukherji, S., and Van Oudenaarden, A. (2009). Synthetic biology: understanding biological design from synthetic circuits. *Nat. Rev. Genet.* 10, 859–871.
- Nemazany, I., Montagnac, G., Russell, R.C., Morzygłod, L., Burnol, A.F., Guan, K.L., Pende, M., and Panasyuk, G. (2015). Class III PI3K regulates organismal glucose homeostasis by providing negative feedback on hepatic insulin signalling. *Nat. Commun.* 6, 8283.
- Nielsen, A.A.K., Der, B.S., Shin, J., Vaidyanathan, P., Paralanov, V., Strychalski, E.A., Ross, D., Densmore, D., and Voigt, C.A. (2016). Genetic circuit design automation. *Science* 352, 352.
- Okamoto, A., Hashimoto, K., Neelson, K.H., and Nakamura, R. (2013). Rate enhancement of bacterial extracellular electron transport involves bound flavin semiquinones. *Proc. Natl. Acad. Sci. U S A* 110, 7856–7861.
- Okamoto, A., Kalathil, S., Deng, X., Hashimoto, K., Nakamura, R., and Neelson, K.H. (2014). Cell-secreted flavins bound to membrane cytochromes dictate electron transfer reactions to surfaces with diverse charge and pH. *Sci. Rep.* 4, 1–8.
- Opgenorth, P., Costello, Z., Okada, T., Goyal, G., Chen, Y., Gin, J., Benites, V., De Raad, M., Northen, T.R., Deng, K., et al. (2019). Lessons from two design-build-test-learn cycles of dodecanol production in *Escherichia coli* aided by machine learning. *ACS Synth. Biol.* 8, 1337–1351.
- Pan, D., Fujimoto, M., Lopes, A., and Wang, Y.X. (2009). Twist-1 is a PPAR δ -inducible, negative-feedback regulator of PGC-1 α in Brown fat metabolism. *Cell* 137, 73–86.
- Prindle, A., Selimkhanov, J., Li, H., Razinkov, I., Tsimring, L.S., and Hasty, J. (2014). Rapid and tunable post-translational coupling of genetic circuits. *Nature* 508, 387–391.
- Ramaswamy, R., González-Segredo, N., and Sbalzarini, I.F. (2009). A new class of highly efficient exact stochastic simulation algorithms for chemical reaction networks. *J. Chem. Phys.* 130, 1–14.
- Sarpeshkar, R. (2010). *Ultra Low Power Bioelectronics: Fundamentals, Biomedical Applications, and Bio-Inspired Systems* (Cambridge University Press).
- Sarpeshkar, R. (2014). Analog synthetic biology. *Philos. Trans. R. Soc. A. Math. Phys. Eng. Sci.* 372, 20130110.
- Sarpeshkar, R., Salthouse, C., Sit, J.J., Baker, M.W., Zhak, S.M., Lu, T.K.T., Turicchia, L., and Balster, S. (2005a). An ultra-low-power programmable analog bionic ear processor. *IEEE Trans. Biomed. Eng.* 52, 711–727.
- Sarpeshkar, R., Baker, M.W., Salthouse, C.D., J. Sit, Turicchia, L., and Zhak, S.M. (2005b). An analog bionic ear processor with zero-crossing detection. In *International Solid-State Circuits Conference*, (IEEE International Digest of Technical Papers. Solid-State Circuits Conference), pp. 78–79.
- Shen, Y., Chen, Y., Wu, J., Shaner, N.C., and Campbell, R.E. (2017). Engineering of mCherry variants with long Stokes shift, red-shifted fluorescence, and low cytotoxicity. *PLoS One* 12, 1–14.
- Stephens, K., Pozo, M., Tsao, C.Y., Hauk, P., and Bentley, W.E. (2019). Bacterial co-culture with cell signaling translator and growth controller modules for autonomously regulated culture composition. *Nat. Commun.* 10, 1–11.
- Stricker, J., Cookson, S., Bennett, M.R., Mather, W.H., Tsimring, L.S., and Hasty, J. (2008). A fast, robust and tunable synthetic gene oscillator. *Nature* 456, 516–519.
- Sturm, O.E., Orton, R., Grindlay, J., Birtwistle, M., Vyshemirsky, V., Gilbert, D., Calder, M., Pitt, A., Kholodenko, B., and Kolch, W. (2010). The mammalian MAPK/ERK pathway exhibits properties of a negative feedback amplifier. *Sci. Signal.* 3, 1–8.
- Teo, J.J.Y. (2019). *Synthetic Analog Feedback Control Circuits in Living Cells*, Ph.D Thesis (Massachusetts Inst. Technol.).
- Teo, J.J.Y., Woo, S.S., and Sarpeshkar, R. (2015). Synthetic biology: a unifying view and review using analog circuits. *IEEE Trans. Biomed. Circuits Syst.* 9, 453–474.
- Teo, J. Kim, J. Woo, S. and Sarpeshkar, R. “Bio-molecular Circuit Design with Electronic Circuit Software and Cytomorphic Chips”, *Proceedings of the IEEE Biomedical Circuits and Systems Conference* (BioCAS 2019), Nara, Japan, pp. 1–4
- Wong, V.W.Y., Stange, D.E., Page, M.E., Buczacki, S., Wabik, A., Itami, S., Van De Wetering, M., Poulosom, R., Wright, N.A., Trotter, M.W.B., et al. (2012). Lrig1 controls intestinal stem-cell homeostasis by negative regulation of ErbB signalling. *Nat. Cell Biol.* 14, 401–408.
- Woo, S.S. (2016). *Fast Simulation of Stochastic Biochemical Reaction Networks on Cytomorphic Chips*, Ph.D. Thesis (Massachusetts Inst. Technol.).
- Woo, S.S., Kim, J., and Sarpeshkar, R. (2015). A cytomorphic chip for quantitative modeling of fundamental bio-molecular circuits. *IEEE Trans. Biomed. Circuits Syst.* 9, 527–542.
- Woo, S.S., Kim, J., and Sarpeshkar, R. (2018). A digitally programmable cytomorphic chip for simulation of arbitrary biochemical reaction networks. *IEEE Trans. Biomed. Circuits Syst.* 12, 360–378.
- Zeng, J., Banerjee, A., Kim, J., Deng, Y., Chapman, T.W., Daniel, R., and Sarpeshkar, R. (2019). A novel bioelectronic reporter system in living cells tested with a synthetic biological comparator. *Sci. Rep.* 9, 1–7.

iScience, Volume 23

Supplemental Information

**The Merging of Biological
and Electronic Circuits**

Jonathan J.Y. Teo and Rahul Sarpeshkar

Supplementary Section I: The Use of Electronic Circuit Software for Biological Circuit Design

We mapped the Bio-OpAmp to its analog circuit equivalent using the mapping discussed in the previous section, and as shown in Fig. 4c. Currents represent molecular fluxes while node voltages represent molecular concentrations. We model transcription and translation using dependent current generators connected in parallel with a resistor and capacitor (RC). The current generators vary their output depending on their voltage inputs, which mimics transcription and translation regulation. This trio of analog parts shown describes a simplified transcription and translation process which we use to model the dynamics of sgRNA, dCas9, LuxI, AiiA and AHL.

The robustness of an electronic OpAmp to manufacturing variations arises when it is used in a closed-loop negative feedback configuration as seen in Fig. 4c. In a Bio-OpAmp, we close the loop by choosing an output molecule that is also the input molecule at its non-inverting terminal, which is AHL in this case. The OpAmp amplifies the difference between input and output, otherwise known as error, to generate an output value. Because the output is fed back into the input, the error value must be small to ensure that after amplification, the output does not create a huge error. The output therefore tracks the non-inverting input signal with an error that is roughly proportional the reciprocal of the OpAmp's open-loop gain if gain is large. It is this reciprocal relationship between gain and error that creates the OpAmp's signature robustness to parameter variations (Sarpeshkar, 2010).

Low sensitivity to parameter variation can similarly be achieved with a Bio-OpAmp. In this case, open-loop gain is a function of catalytic efficiency, dissociation constant, degradation rate and the steady-state concentration of the underlying biomolecules. By applying small-signal circuit analysis to the analog circuit in Supplementary Fig. 4 (Sarpeshkar, 2010), we recover the precise relationship between loop gain and biological parameters (See (Zeng et al., 2018)). Since an OpAmp is robust to variations in open-loop gain if its value is much greater than 1, we can 'spread' the uncertainty to parameters that are difficult to control and tune the controllable parameters to generate a large overall loop gain. One other important consideration that applies specifically to the Bio-OpAmp is that biochemical reactions are generally sigmoidal. If the concentration of a particular biomolecule is operating close to saturation, it responds more slowly to change, therefore reducing loop gain and attenuating negative feedback. To reduce sensitivity, the Bio-OpAmp should operate at a level where its constitutive molecules have concentrations that are close to their respective dissociation constants in order to maximize open-loop gain.

A classical OpAmp is often employed in electronic circuits because of its resistance to upstream and downstream loading effects i.e. connecting an OpAmp to an existing circuit does not affect either the circuit or the OpAmp's original behavior. In synthetic biology, loading effects are often called retroactivity and they are known for introducing context-dependent effects to

otherwise well characterized synthetic circuits (Del Vecchio et al., 2008). For example, a repressor in a naïve feedback circuit binds to an upstream promoter to create negative feedback (Stricker et al., 2008), but a cognate promoter downstream that is placed on a high copy plasmid acts like a shunt that competes for the same repressor, thereby attenuating the strength of the negative feedback. In contrast, the Bio-OpAmp rejects the downstream disturbance by leveraging its high open-loop gain to attenuate the ‘error’ such that the output is determined only by input Arabinose. Additionally, the third gain stage is designed to be fast so that LuxI and AiiA can respond to downstream changes of AHL quickly. Fast dynamics, combined with high open-loop gain, are responsible for the low output impedance of the Bio-OpAmp. As for the input signal, the low copy number of araC in the first stage of the Bio-OpAmp ensures that the upstream concentration of Arabinose is not affected by its use-it-and-lose-it binding. Low araC copy number is therefore responsible for the high input impedance of the Bio-OpAmp

One potential problem with multi-stage OpAmps in negative- feedback loops is the occurrence unintended oscillation caused by large open-loop gains. In Bio-OpAmps, the problem is further compounded by delays from binding, transcription and translation initiation and diffusion of molecules. Intuitively, delays and phase shifts are well-known for causing oscillations in otherwise stable systems because they prime a feedback loop to overcorrect an initial disturbance due to a delay in response, and the overcorrection triggers another round of correction in the opposite direction through feedback, therefore creating oscillation (Sarpeshkar, 2010). To attenuate oscillations, we could reduce open-loop gain at the expense of increasing tracking error and reducing OpAmp performance. An alternative solution commonly employed in analog electronic circuit design is to introduce a dominant pole by slowing the time scale of one of the stages. We achieve the slowdown in the second stage of the Bio-OpAmp by leveraging the relatively slow process of protein translation compared to RNA transcription and small-molecule synthesis.

When designing the Bio-OpAmp, we modeled and simulated the analog circuit equivalent (see Fig. 4) with the circuit software tool, Cadence, a computer aided design (CAD) tool. Cadence converts the schematic into a system of discrete-difference numerical equations that it simulates on a CPU through well-known and fairly advanced numerical-analysis techniques, honed over decades to improve convergence. It derives implicit relationships between voltages and currents by applying the laws of conservation of charge so users can avoid the error-prone process of accounting for reaction fluxes manually. We can change the topology simply by connecting wires between circuit motifs and replacing components with the click of a button. Using the suite of analysis tools in Cadence, we performed frequency analysis to identify sources of instability in Bio-OpAmp and eliminated them using the dominant-pole compensation technique from analog circuit design (Sarpeshkar, 2010). We were able to arrive at our final Bio-OpAmp design because we adopted an analog circuit framework and were able to leverage its many tools and concepts.

Supplementary Section II: Compiling Circuits

To simulate any transcription-translation network on the transistor-based cytomorphic chips, we first create a mapping for the RC circuit motif of the Bio-OpAmp (See Supplementary Fig. 6 and Supplementary Fig. 7) (Sarpeshkar, 2010, 2014; Teo et al., 2015). Each cytomorphic block on the chips is designed to produce a current flux given by a general bidirectional (A + B) → (C+D) reaction with C being capable of being independently produced or degraded by other reactions. It is parametrized and modeled by the following equation:

$$\text{Rate} = k_r \left(\left((A_{tot} - C_{tot}) \left(\frac{B_{tot} - C_{tot}}{KD_{fw}} \right)^n + C_{prod} \right) - \left(\frac{C_{free} D_{free}}{KD_{rv}} \right) \right) - K_{deg} \left(\frac{C_{free} (ratC)}{I_{One}} + C_{deg} \right) \quad \text{Eq. 1}$$

$$= ((\text{forward reaction}) - (\text{reverse reaction})) - (\text{degradation rate})$$

where $A_{tot} - C_{tot} = A_{free}$ and $B_{tot} - C_{tot} = B_{free}$ if C (or D) can only be produced by a reaction involving only A and B (Woo et al., 2018). Supplementary Fig. 7 shows how the cytomorphic circuit building blocks can be wired to simulate a transcription-translation reaction. The configuration shown here can be viewed as a variant of the Michaelis-Menten (MM) enzyme-substrate binding configuration for protein blocks that is described in Fig. 2 of (Woo et al., 2018): It assumes that the substrate concentration is much larger than enzyme concentration such that substrate depletion is negligible. This assumption works because the number of transcription factors (the ‘substrate’) is much larger than the number of binding sites for the transcription factor on DNA (the ‘enzyme’). To emulate the lack of substrate depletion explicitly, we open the use-it-and-lose-it feedback loop that connects C_{tot} to B_{tot} . To reduce the number of parameters and improve model interpretability, we typically use normalized variables, i.e., variables wherein substrate concentrations are divided by their respective dissociation constants.

One major difference between $ES \rightarrow P$ catalysis and transcription-translation is that the transcription factor (S) is not directly consumed when it activates the production of RNA transcripts and proteins letting us model transcription networks simply and efficiently. To emulate this condition on the chip, we can remove the use-it-and-lose-it feedback loop between S and P so that they are no longer coupled. If we wish to study the more complex effects of loading and resource consumption exactly in the circuit, i.e., the effects of the substrate depletion on downstream variables and their back action on the substrate, we can re-instate such use-it-and-lose-it negative-feedback loops (Teo et al. 2015, Sarpeshkar, 2010, Sarpeshkar 2014, Woo et al. 2018).

Next, we use a conductance-divider circuit to model competitive binding between 2 or more substrates (See Supplementary Figs. 8 for a circuit instantiation using dCas9 and sgRNAs, which

is directly relevant to the Bio-OpAmp). In a classical conductance-divider circuit, conductances are connected in parallel such that they divide an input current into multiple fluxes in a weighted fashion, with weights proportional to the conductance. The value of each conductance is set to its respective normalized substrate concentration. An additional conductance with value 1 is used to account for the amount of free enzyme. The current fluxes represent the proportion of enzymes that are bound or unbound at steady state, and they obey the following equation

$$I_x = E_{\text{tot}} \frac{\frac{X}{K_{dx}}}{1 + \frac{S1}{K_{ds1}} + \frac{S2}{K_{ds2}}} \quad \text{Eq. 2}$$

where X is either $S1$ and $S2$. To model the dynamics of enzyme substrate binding, we can add a capacitor in parallel to the conductance divider. To model competition between more substrate species, we simply add a conductance for each additional substrate. The circuit can be mapped onto the cytomorphic chip using a variant of the fan-out configuration described in Fig. 7b of (Woo et al., 2018). Just like the transcription-translation motif, we assume that $S \gg E$ so we can ignore substrate depletion by removing the use-it-and-lose-it feedback loop, as shown in Supplementary Fig. 8. To increase the number of competing substrates, we simply add a new protein block for each additional substrate and subtract bound ES complexes from E_{Tot} .

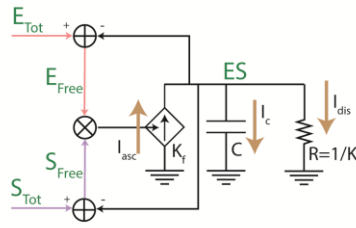
Finally, we need a circuit motif to model the third differential gain stage of the Bio-OpAmp of Fig. 4. The enzymes, LuxI and AiiA synthesize and degrade the AHL molecule respectively, which is modeled by using a current generator that is controlled by LuxI and a degradation resistor that is controlled by AiiA as shown in Supplementary Fig. 9a. The cytomorphic instantiation as shown in Supplementary Fig. 9b converts the reverse reaction from Eq. 1 to a degradation reaction.

Supplementary Section III: Simulation results from cytomorphic chips

From small-signal analysis (See Supplementary Fig. 4), the Bio-OpAmp has a feedback gain of $f = A/B$, where A and B are the DC gains of the AHL and Arabinose sensing pathway respectively. Consequently, the closed-loop gain of the Bio-OpAmp is approximately $1/f = B/A$ when open-loop gain is large. A high throughput 2D sweep of DC gains A and B on the chip reveals a B/A dependence between input Arabinose and output AHL as shown in Supplementary Fig. 13. It should be noted that the closed loop gain is derived from the linearization of the circuit, and is therefore valid over a limited range of input Arabinose. Beyond this range, non-linear behavior such as saturation dominates, again pointing to the importance of using negative feedback with high loop gain for faithful tracking of the set point of a system.

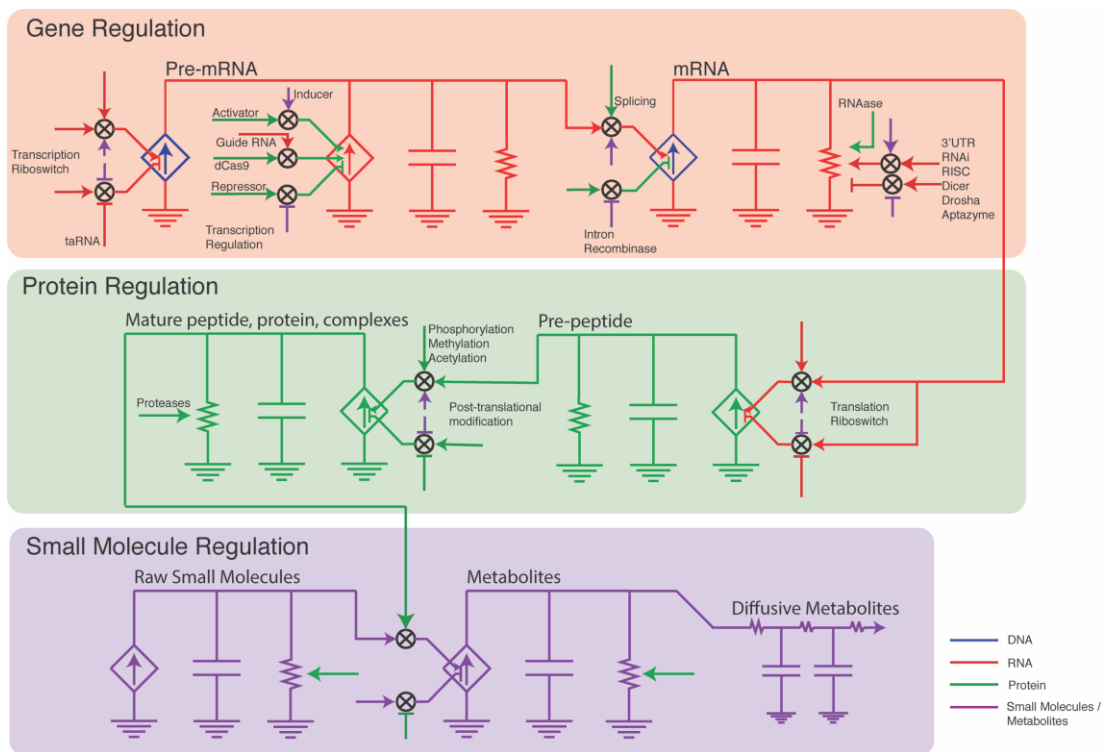
As we alluded to in the previous section, the second amplification stage utilizes the competition between sgRNA1 and sgRNA2 for dCas9 to increase gain. To optimize the strength of

amplification, we performed a 2D sweep on the dissociation constants between sgRNAs and dCas9. Supplementary Fig. 12 shows that differential gain is maximized when both dissociation constants are the same. When one of the sgRNA concentration increases while the other stays constant, it not only forms more complexes with dCas9, it also displaces the other sgRNA from dCas9, thus creating a push-pull reaction. If the binding affinities of both sgRNAs are similar, the symmetry ensures that there is an equal concentration of dCas9-sgRNA1 and dCas9-sgRNA2 such that any change in either sgRNA concentrations will elicit a stronger push-pull effect than if the concentration of complexes were disproportionate. Another observation is that a stronger binding affinity increases differential gain. In the presence of a large concentration of unbound dCas9, increases in either sgRNA concentrations would increase binding to unbound dCas9 copies instead of the bound complexes. The unbound dCas9 therefore acts as a buffer that attenuates gain. By increasing binding affinity, we ensure that most dCas9 are bound to sgRNA, therefore reducing their buffering capacity.

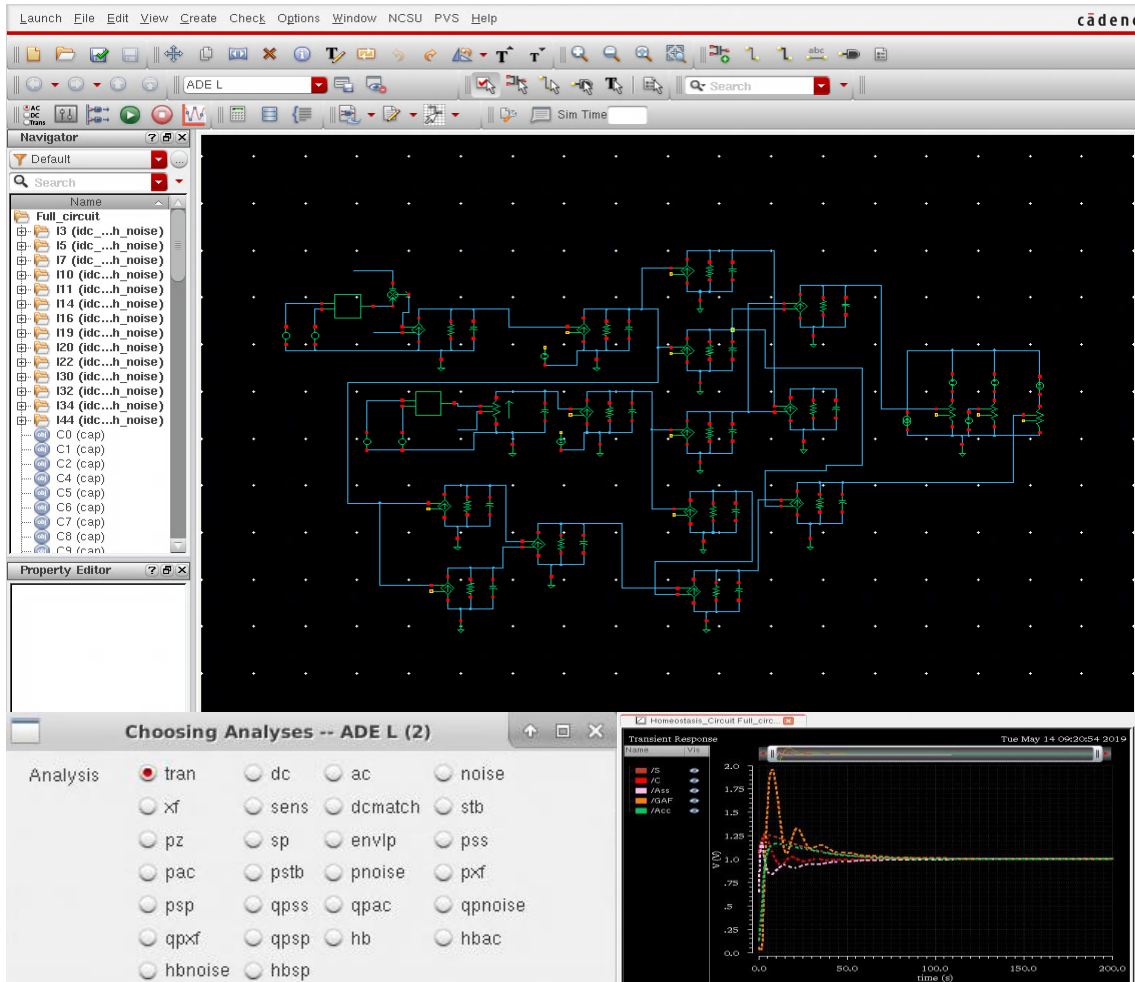


$$\begin{aligned}
 I_{dis} &= \frac{ES}{R} = K_r * ES & \frac{dES}{dt} &= \frac{1}{C} \frac{dq}{dt} \\
 I_{asc} &= K_f * E_{Free} * S_{Free} & &= \frac{I_{asc}}{C} - \frac{I_{dis}}{C} \\
 \frac{dq}{dt} &= I_c = I_{asc} - I_{dis} & &= \frac{I_{asc}}{C} - \frac{ES}{CR} \\
 ES &= \frac{1}{C}q & &= \frac{K_f}{C} * E_{Free} * S_{Free} - \frac{K_r}{C} * ES \\
 & & &= K'_f * E_{Free} * S_{Free} - K'_r * ES
 \end{aligned}$$

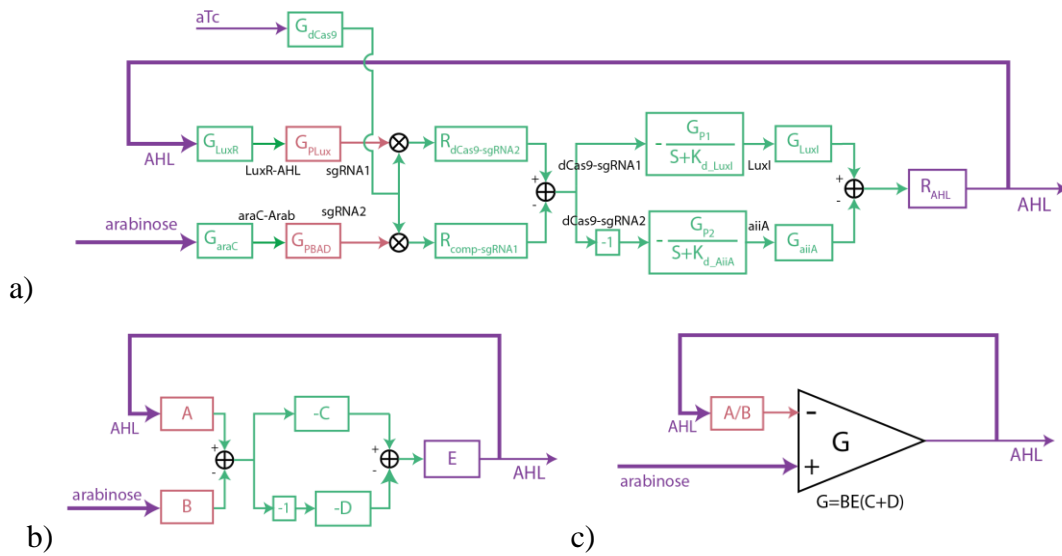
Supplementary Fig. 1. Dynamics of the circuit of Fig. 2 that models an enzyme-substrate binding reaction. Related to Section I. The circuit reproduces the dynamics of an enzyme-substrate binding reaction. Voltages are analogous to molecular concentration and represented in green text. Currents are analogous to molecular flux. Using Kirchhoff's current law, the current flowing into the capacitor, I_c , is the difference between I_{asc} and I_{dis} . If the rate of association is greater than the rate of dissociation, a positive I_c flows into the capacitor (C) and causes an accumulation of charge (q) which increases the voltage ES. When I_c is zero, ES stays constant and the system is in equilibrium. I_{asc} is a second-order association reaction which depends on the product of voltages E_{free} and S_{free} . We use voltage adders to generate the free quantities and a voltage multiplier to calculate their product. The dependent current generator, represented by a diamond symbol, scales the input voltage by K_f to produce I_{asc} . I_{dis} is a first-order reaction representing dissociation. We model the first-order behavior using a simple resistor that depends on the reciprocal of K_r .



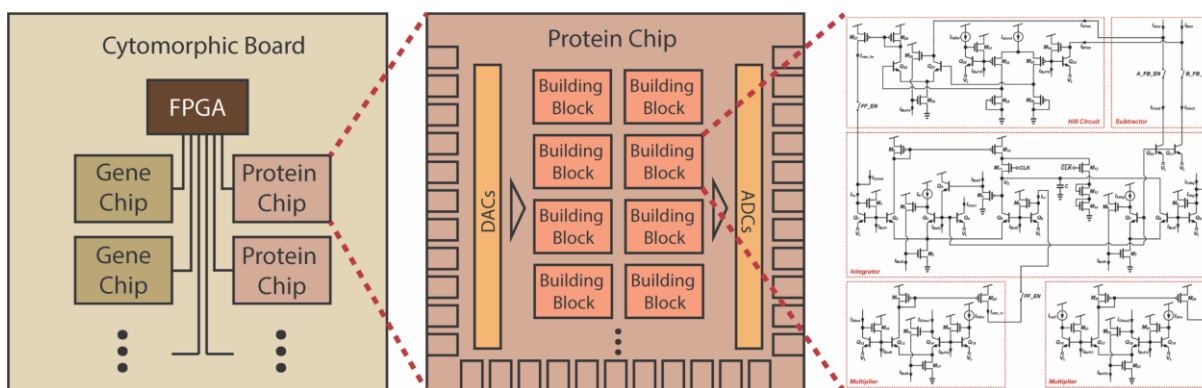
Supplementary Fig. 2. Canonical Analog Circuit that represents DNA, RNA, Protein, and Small-Molecule Circuits in Molecular Biology. Related to Section I. The canonical circuit schematic represents biological reactions involving DNA (blue), RNA (red), protein (green) and small-molecules/metabolites (purple). It contains sub-circuits for transcription, translation and various forms of regulations including ribosomal switches, transcription factors, splicing, post-translational modification and CRISPR-based regulation. Portions of this circuit have been instantiated in 17 synthetic biological circuits over 20+ years and have shed insight into their operation (Teo et al., 2015).



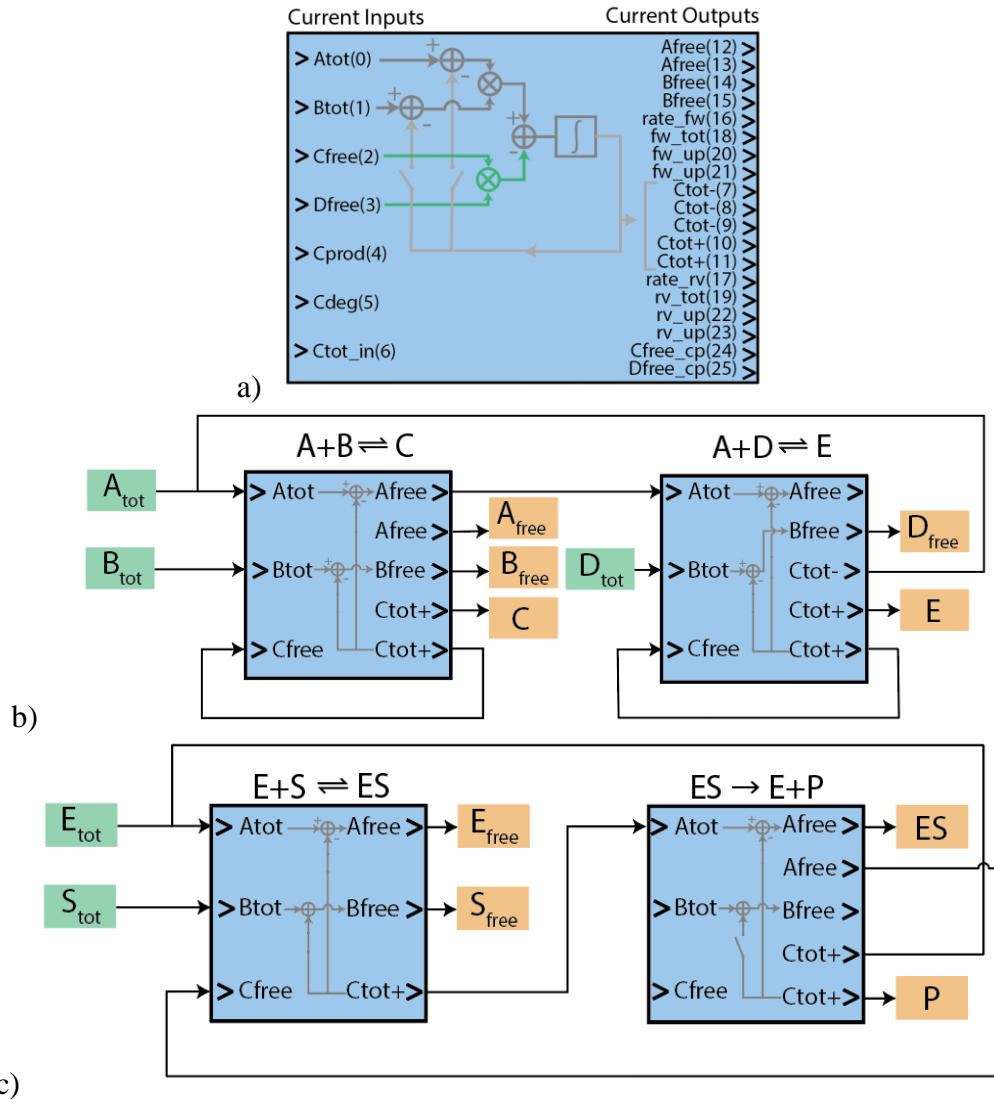
Supplementary Fig. 3. Cadence – An analog electronic circuit Computer Aided Design (CAD) software tool. Related to Section II. This software tool includes a suite of 26+ forms of analysis that have been used over decades to design extremely complex integrated circuits with billions of transistors that meet important system performance specifications involving speed, accuracy, power efficiency, robustness, and device count or chip size.



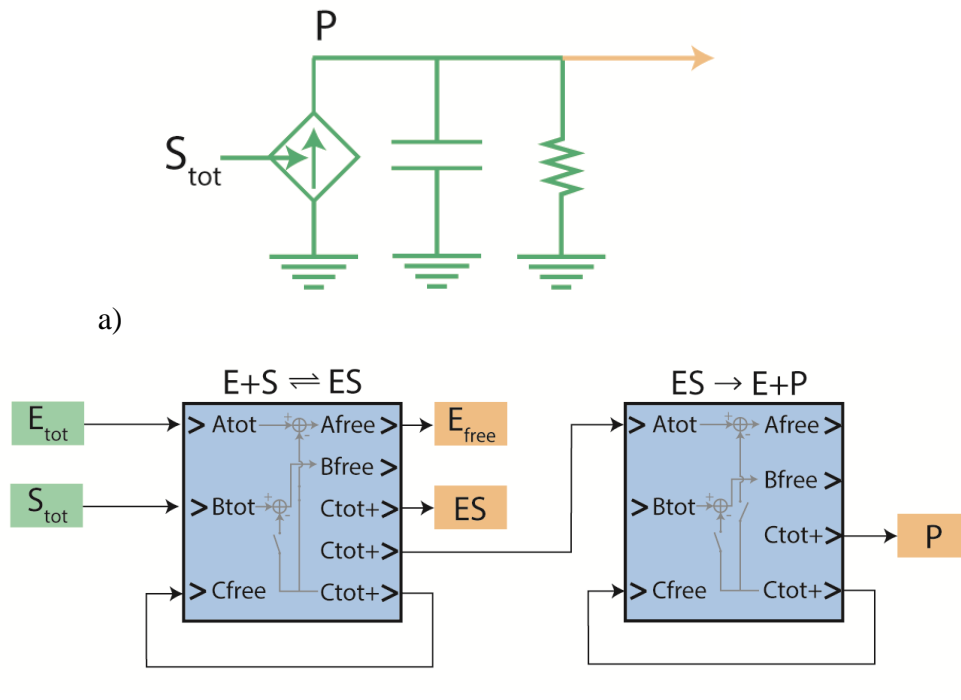
Supplementary Fig. 4. Small-signal analysis of the Bio-OpAmp. Related to Section III and Fig. 4. a) A small-signal schematic of the Bio-OpAmp with detailed gains corresponding to different parts of its circuit. b) A small-signal schematic with aggregated gains. c) A small-signal schematic that further aggregates gains into one open loop gain G and a feedback loop gain A/B of a closed-loop operational amplifier. The hierarchical simplifications of the gains in a Bio-OpAmp from a) to c) illustrate how many gains or parameters in a biological circuit or system can collapse into only 1 or 2 effective parameters that are important.



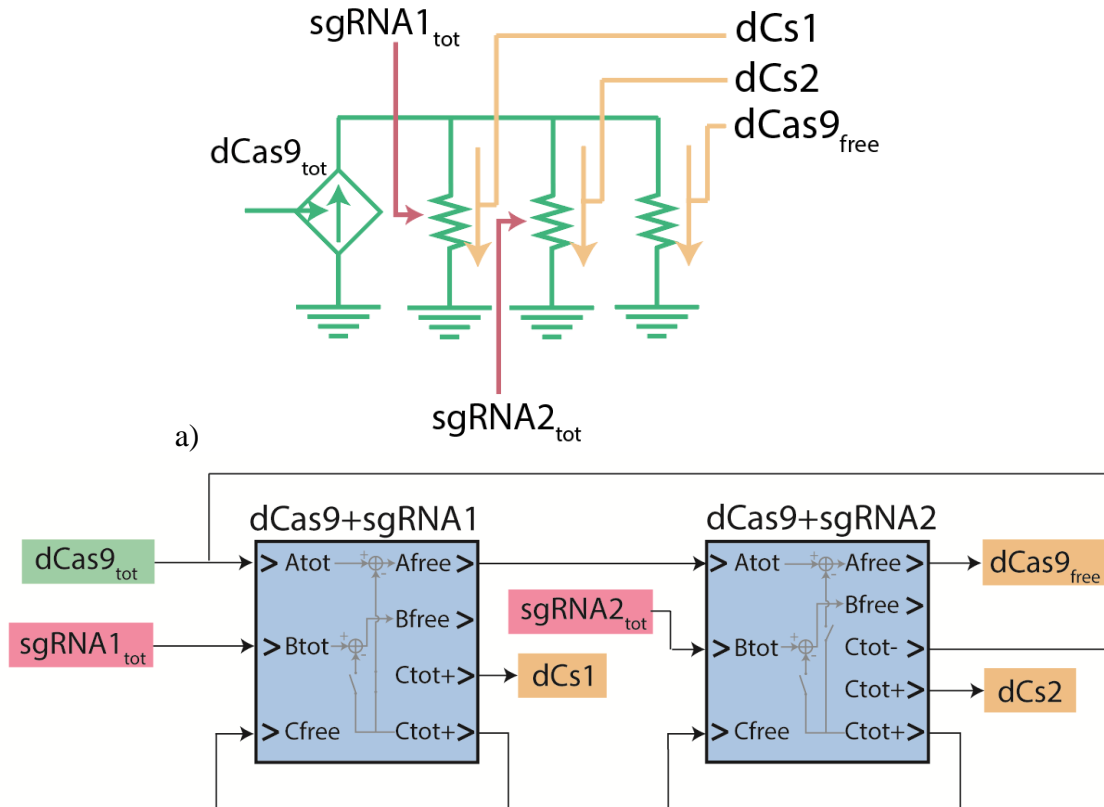
Supplementary Fig. 5. Cytomorphonic systems architecture. Related to Section III and Fig. 5. Overall architecture of the hardware of a typical cytomorphonic system implemented on an electronic printed circuit board. On such a board, many cytomorphonic chips (e.g., gene chips and protein chips) are connected to one another via an FPGA to run massively parallel simulations of stochastic biochemical reaction networks. Both of the cytomorphonic chips contain various reconfigurable building-block circuits that are digitally programmed to model and simulate various cell functions. Reconfiguration of their parameters and intra-chip connectivity is achieved by electronic currents created by DACs and digital bits that are stored in memory. Routing channels convey electronic currents that represent state variables from one block to another to enable programmable network connectivity via digital switches. ADCs are used to read out the value of state variables. Gene chips have mass action and Michaelis-Menten reaction blocks, Hill blocks, ITD blocks, analogic DACs, gain and time constant blocks, and stochastic circuits. Protein chips have protein chemical-reaction blocks and stochastic circuits. A protein block is shown in the rightmost subfigure as an example. Further details are described in (Woo et al. 2015) and (Woo et al. 2018).



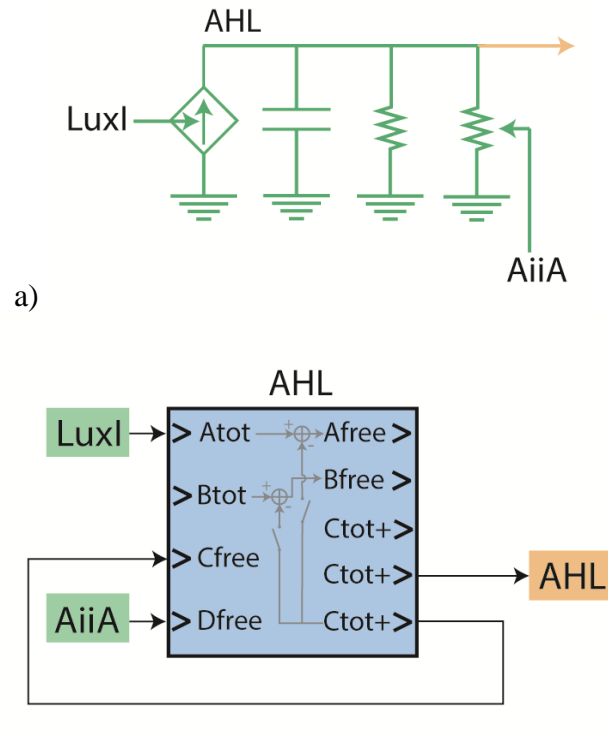
Supplementary Fig. 6. Examples of multiple configurations of protein blocks on cytomorphic chips that can simulate various biochemical reactions. Related to Section III and Fig. 6. a) Each chip contains multiple protein blocks with current input and output ports as shown in the figure. Embedded within the blocks are multiple switches and Digital-to-Analog Converters (DACs) to customize biochemical network parameters. Back-propagation of downstream effects to upstream reactions due to use-and-lose-it feedback loops in non-modular cascades of reactions are also accurately represented. b) To simulate a fan-out reaction, we connect two protein blocks as shown in (Woo et al., 2018). The first block simulates the binding between A and B. The second block accounts for binding between A and C. c) To simulate an enzyme-substrate catalytic reaction, one block is used to model the formation of the enzyme-substrate complex. A second block captures the molecular dynamics and molecular production/conservation inherent in substrate-to-product conversion.



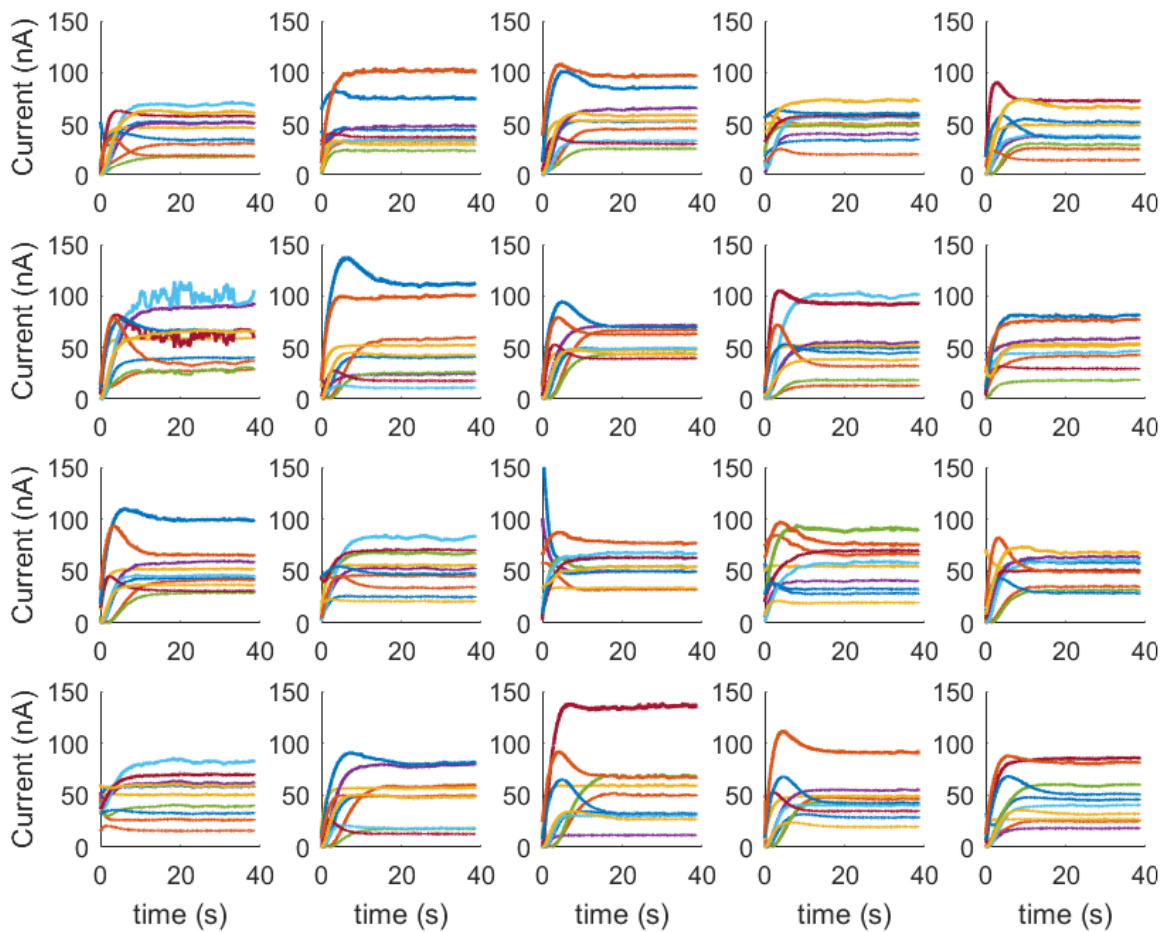
Supplementary Fig. 7. Simulation of a combined transcription-and-translation block with cytomorphic-chip protein blocks. Related to Section III and Fig. 6. (a) The circuit motif shown above is the same as a commonly repeating circuit motif in the microbial Op-Amp circuit model corresponding to Fig. 4c. (b) The cytomorphic configuration of protein blocks shown above is a modification of a Michaelis-Menten configuration described in (Woo et al., 2018). It is convenient for compilation of Fig. 4 circuit motifs (motif in (a)) to equivalent cytomorphic circuit motifs as shown here (cytomorphic circuit motif in (b)). Since, in this simplified circuit motif, the production of protein P does not affect input concentration S_{TOT} but is only controlled by it, use-it-and-lose-it feedback loops in the first protein block corresponding to S and in the subsequent reaction block corresponding to ES are absent. Overall, the production of P from the second protein block does not affect the first protein block and compiles the circuit shown in (a) to a cytomorphic equivalent shown in (b).



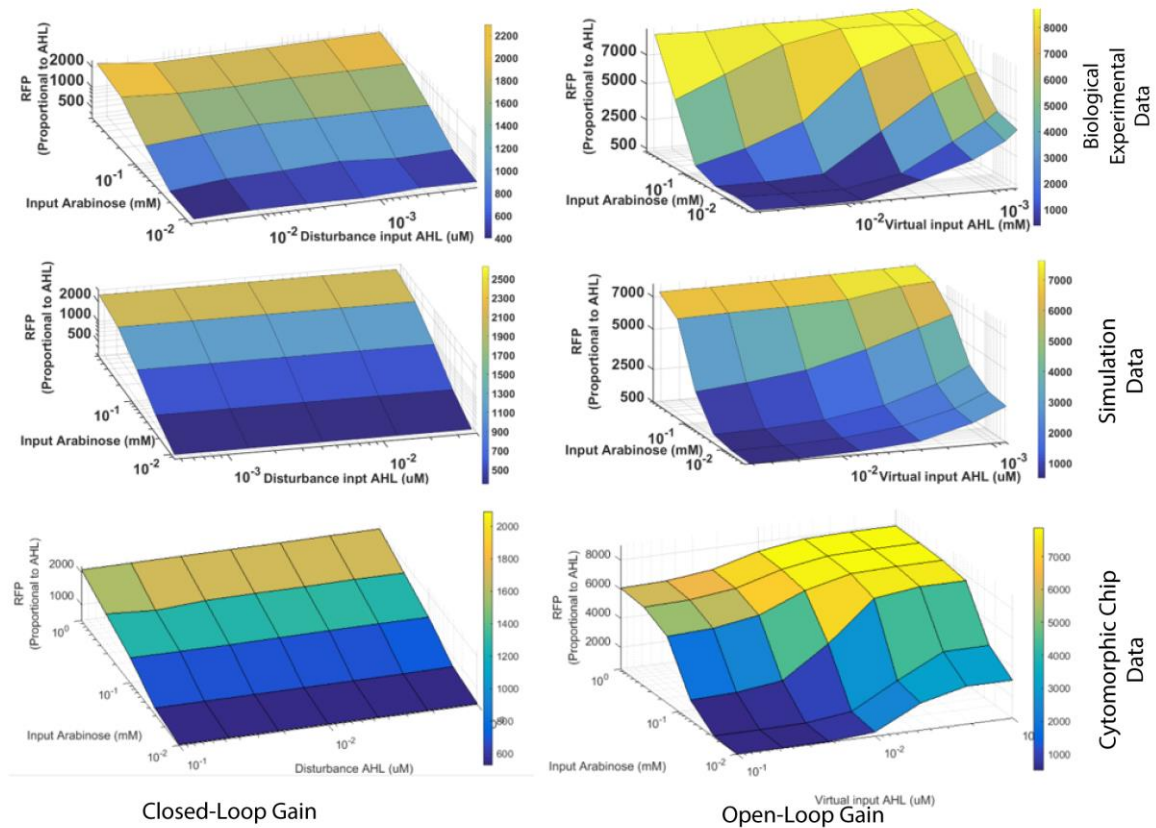
Supplementary Fig. 8. Simulation of a fanout circuit motif block with cytomorphic-chip protein blocks. Related to Section III and Fig. 6. (a) The conductance-divider circuit motif shown above is the same as that in the microbial Op-Amp circuit model corresponding to Fig. 4c that models competitive binding of *dCas9* to *sgRNA1* or *sgRNA2*. Each conductance represents the normalized concentration of *sgRNA1* or *sgRNA2*, and the current flux through each conductance represents the amount of bound *dCas9* respectively. A third conductance of value 1 accounts for the proportion of unbound *dCas9*. (b) Each cytomorphic circuit block calculates the amount of enzyme bound to either *sgRNA1* (*dCs1*) or *sgRNA2* (*dCs2*) respectively, accounting for accumulating depletion in *dCas9* when bound, in a cascade.



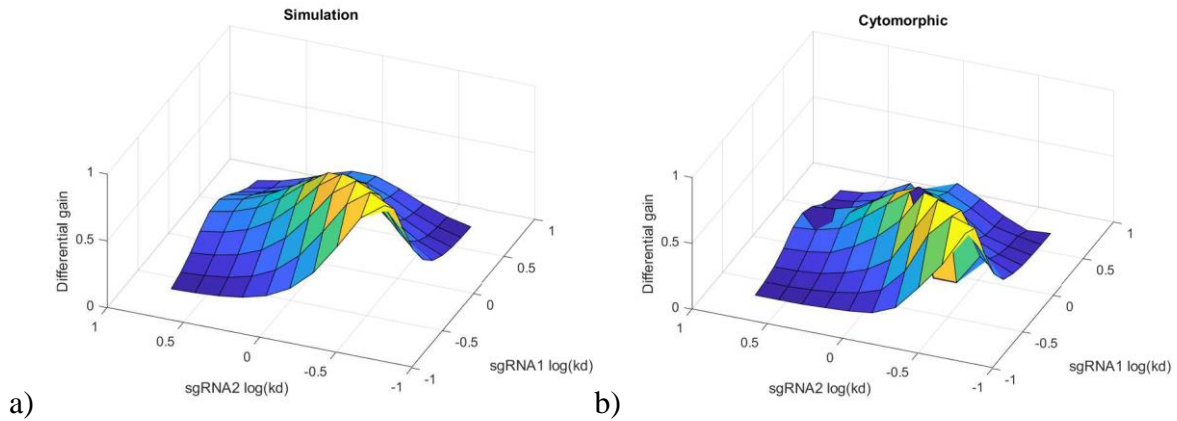
Supplementary Fig. 9. Simulation of a production-degradation circuit motif block with cytomorphic-chip protein blocks. Related to Section III and Fig. 6. a) The production-degradation circuit in (a) contains dependent current generators that produce *AHL* or degrade *AHL* in proportion to the amount of *LuxI* or *AiiA* respectively. (b) To simulate production, the cytomorphic circuit equivalent uses a first-order forward reaction with *LuxI* corresponding to *Atot* and no use-it-and-lose-it feedback (species *A* has no feedback that is dependent on *C* and species *B* is constant). To simulate degradation, the cytomorphic circuit equivalent uses a second-order reverse reaction that depends on *AiiA* (corresponding to species *D*) and *AHL* (corresponding to species *C*). Finally, the cytomorphic circuit block also allows programmable constitutive degradation of *C* if needed, which is also present in the circuit motif of (a). Thus, all elements of the motif of circuit (a) can be implemented in just the single cytomorphic circuit block of (b).



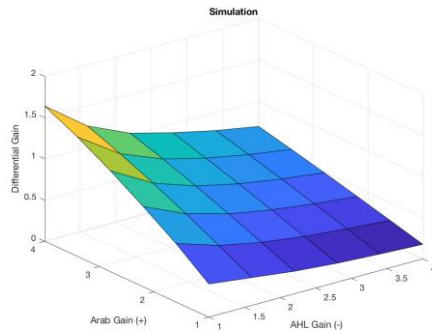
Supplementary Fig. 10. Parallel dynamical simulations of Bio-OpAmp on cytomorphic chip. Related to Section III. Multiple instances of the Bio-OpAmp were simulated in parallel with stochastics to facilitate analysis such as parameter optimization, sensitivity analysis and stability analysis.



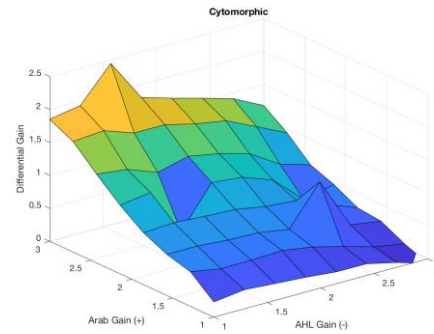
Supplementary Fig. 11. Comparison of steady-state input-output Bio-OpAmp characteristics in biological experiments (Zeng 2018 et al.), circuit software simulation, and cytomorphic chip simulation. Related to Section III. (Left) Closed-loop data; (Right) Open-loop data. RFP corresponds to fluorescent measurements of an output proxy molecule that corresponds to output AHL concentration. Good agreement is seen in all three cases: Unlike the Closed-loop data, the Open-loop RFP output data does not track the input setpoint *Arabinose* molecule concentration in a proportional fashion but is highly sensitive to it. Similarly, unlike the Closed-loop data, the Open-loop data does not reject the disturbance input AHL but is highly sensitive to it.



Supplementary Fig. 12. Symmetric K_d of *sgRNA1* and *sgRNA2* improves differential gain. Related to Section III. a) Software simulation. b) Cytomorphic chip simulation. The Bio-OpAmp leverages the competition between *sgRNA1* and *sgRNA2* with *dCas9* to improve its open-loop gain. Such competition uses a well-known concept in analog circuit design called push-pull amplification (Sarpeshkar 2010). Push-pull amplification works optimally if the push and pull arms have symmetric strengths such that small-signal parameters for open-loop gain are not determined by the worst-case performance of a saturated non-optimal arm. In the context of the Bio-OpAmp, we can tune the dissociation constant of both guide RNAs to be the same to maximize differential gain. We show using both software and chip simulation that the differential gain is indeed highest when both dissociation constants are the same. As in the Bio-OpAmp, in nature, push and pull amplification is also seen in feedback regulation of glucose via insulin (pull) or glucagon (push).

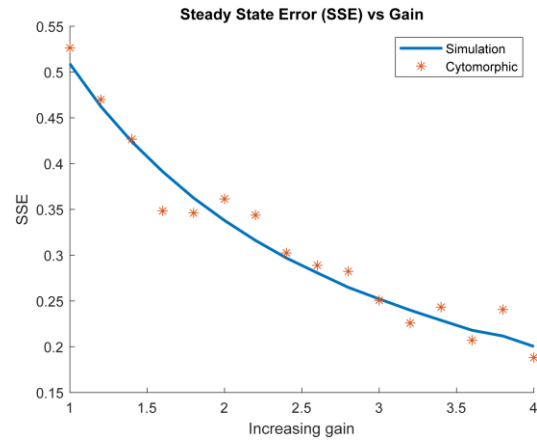


a)



b)

Supplementary Fig. 13. Closed-loop gain with varying gain of Arabinose and AHL. Related to Section III. a) Circuit software simulation. b) Cytomorphic chip simulation. In the Bio-OpAmp, the feedback loop gain is determined the small-signal gain of AHL/Arabinose. The Closed-loop gain of the Bio-OpAmp changes in proportion to the reciprocal of the feedback loop gain.



Supplementary Fig. 14. Steady-State Error vs Gain in a Bio-OpAmp. Related to Section III. The steady-state tracking error of a closed-loop Bio-OpAmp scales like $1/(1 + G)$ in the presence of negative feedback, where G is the differential gain of the operational amplifier. As gain increases, the steady-state error drops as predicted and confirmed via simulations in software and on cytomorphic chips.